修 士 論 文 の 和 文 要 旨

研究科・専攻	大学院　情報理工学研究科　情報・ネットワーク工学専攻　博士前期課程		
氏　　名	原　郁紀	学籍番号	1731129
論 文 題 目	非直交多元接続のための高信頼空間変調		

要　旨

マルチユーザ空間変調（SM: Spatial Modulation）では，SM 信号の疎性を用いた圧縮センシングによるマルチユーザ検出が研究されているものの，受信機においてチャネル情報が完全に既知であるという条件の下で議論されている．実際には受信機側でチャネル情報を推定し，推定したチャネル情報を用いて復調処理を行う．推定したチャネル情報の精度は復調の精度に影響を及ぼすため，チャネル推定は重要なものであり考慮しなければならない．

そこで本研究ではチャネル推定を，ブロックスパース性を有する信号の再構成問題として扱い，ブロックスパース性を考慮した複素数近似メッセージ伝播法（BS-CAMP: Block-Sparse Complex Approximate Message Passing）によって信号の再構成を行う方法を提案する．BS-CAMP は受信機が送信信号に含まれる非零要素の個数を事前に知る必要がない再構成アルゴリズムとなっており，ランダムアクセス方式にも適用可能である．計算機シミュレーションより，BS-CAMP によるチャネル推定の精度やスループット特性への影響を示す．

さらに，高信頼な通信を実現するにはチャネル推定だけでなく誤り訂正符号が重要となる．そこで併せて本研究では SM に誤り訂正符号化を組み合わせたものの一つである，ターボトレリス符号化空間変調（SM-TTC: SM with Turbo Trellis-Coding）における符号の最適化及び性能解析を行った．具体的には，シンボルベース EXIT（EXtrinsic Information Transfer）チャートを用いた低演算符号探索法によって，演算量を低減しながら最良の特性を示す符号を探索する．計算機シミュレーションより，探索した符号を用いた SM-TTC が従来のものよりも優れていること，および提案手法が従来の符号探索法よりも低計算量で符号探索が可能であることを示す．

平成30年度　修士論文

Highly-Reliable Spatial Modulation for Non-Orthogonal Multiple Access

非直交多元接続のための高信頼空間変調

学籍番号　1731129

氏　名　原　郁紀

指導教員　石橋　功至 准教授

電気通信大学　情報理工学研究科

情報・ネットワーク工学専攻

提出日　平成31年3月14日

Abstract

For multiuser spatial modulation (SM) systems, multiuser detection based on compressed sensing exploiting the inherent sparsity of SM signals has been studied and discussed under the assumption that the receiver knows the channel state information (CSI) perfectly. In practice, the perfect CSI is not available even at the receiver, and thus the channel estimation is essential for detection. The accuracy of channel estimation determines the accuracy of the signal detection, so that the channel estimation is a crucial task for wireless communications. From these backgrounds, we propose *block-sparse complex approximate message passing* (BS-CAMP) algorithm for the channel estimation of multiuser SM system and evaluate the normalized mean squared error of CSI obtained by BS-CAMP and the throughput of multiuser SM systems with proposed estimation via computer simulations. Furthermore, even if the perfect CSI is available, the performance of SM systems is significantly limited by spatial correlation of channels. To overcome this problem, we focus on applying turbo trellis-coding to SM systems. In order to optimize SM with turbo trellis-coding (SM-TTC), we propose a low-complexity code search method for SM-TTC using the symbol-based extrinsic information transfer (EXIT) charts. We also confirm that SM-TTC using the code obtained by proposed search outperforms the conventional one and that the computational complexity of the proposed search is lower than conventional search, via computer simulations.

Contents

List of Figures

List of Tables

Chapter 1

Introduction

This thesis describes comprehensive studies on wireless communication systems based on spatial modulation (SM) for multiuser and highly-reliable communications. This chapter firstly introduces the research backgrounds and the technical challenges. After we have stated research motivations and contributions, we give the organization of this thesis.

1.1 High Requirements of Future Applications

With the rapid development of the mobile communication system and the widespread use of smartphones, mobile data traffic has been grown explosively. On the other hand, new services and applications impose high requirements such as data rate, low latency, and so on. Therefore, in the fifth generation (5G) mobile communication system, three main usage scenarios are envisioned [1]:

- **Enhanced mobile broadband (eMBB)**
- **Massive machine type communications (mMTC)**
- **Ultra-reliable and low latency communications (URLLC)**

The illustration of usage scenarios of International Mobile Telecommunications (IMT) for 2020 and beyond is shown in Fig. 1.1. These usage scenarios reflect user and application trends to continuously evolve every life by mobile devices, e.g., human-centric communication and machine-centric communication. The usage scenarios suppose the applications requiring massive connectivity, e.g., internet of things (IoT), and applications demanding both high data rate and low latency such as three-dimension (3D) video, augmented-reality (AR), and virtual-reality (VR). These applications have been expected to provide a significant impact on services such as deliver education, health care, and so on [2, 3, 4].

However, we face a critical problem: trade-off between throughput and system complexity in wireless communication systems. In wireless communications, multiple-input-multiple-output (MIMO) system takes an important role as the benefits of the improvement the bandwidth efficiency. Therefore, the MIMO system is one of the development areas for 5G systems, e.g., massive MIMO and beam-forming [2]. However, the MIMO systems in practice have significant challenges: the complexity of signal processing and the energy consumption of radio frequency (RF) chains at each mobile device.

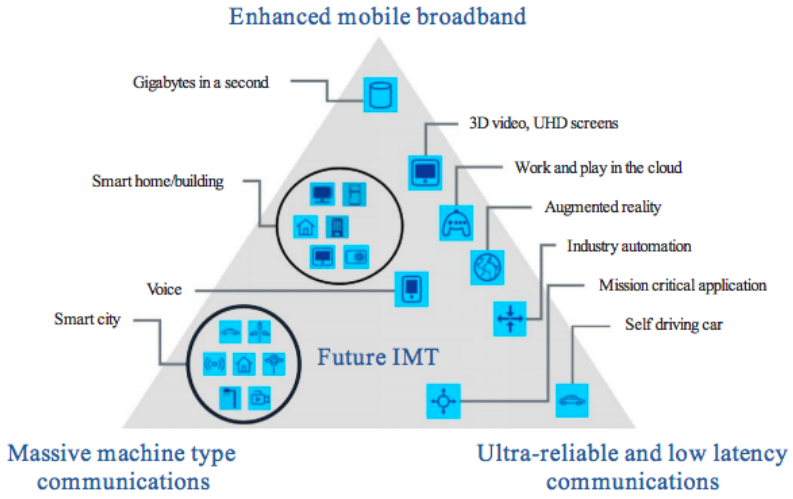

Figure 1.1: Usage scenarios of IMT for 2020 and beyond [1].

Table 1.1: Wireless network requirements for some future applications [2].

Wireless network requirement	VR and AR applications	Smart city applications	
		Traffic management	Emergency services support
Very high throughput/connection	5	4	4
Very low latency	5	3	4
Very high bandwidth density	3	3	4
Very high connection density	1	3	3
Very low device power	1	4	1

1.2 Focus of This Thesis

In the former section, we introduced the applications requiring low latency, high data rate, and massive-connectivity, and especially dealt with IoT, AR, VR, etc. as promising applications to improve the quality of life.

Table 1.1 summarizes the wireless network requirements for future applications based on reference [2], where the level of importance is expressed as 5 = extremely important and 1 = not very important. VR and AR applications and smart city applications can be treated as the kind of eMBB and mMTC services, respectively. This table indicates that major requirements on these applications can be described as below:

1. **High throughput** (for eMBB and mMTC)
2. **Low latency** (for eMBB and mMTC)
3. **High connection density** (for mMTC)

In this thesis, we focus on the above requirements.

The fundamental challenge of mMTC services is to establish an efficient scheme to support a massive number of devices. In IoT applications, only a small number of devices among existing them is randomly active because of the sporadic device-activity. This occurs due to the system design that devices are only activated when triggered by external events, like a sensor network. In these scenarios, not only the reception of their data but also the identification of active users are required. Therefore, the channel estimation and the user identification are key challenges since these accuracies influence whether data are received correctly. On the other hand, both the spectrum efficiency and reliability are essential for achieving very high throughput. In general, an error-correcting code guarantees high reliability of data reception, hence its design is significant in the services as well as conventional wireless communication systems.

The focused requirements have motivated many researchers to discuss multiple access schemes, i.e., non-orthogonal multiple access (NOMA) [5], MIMO techniques, and so on. In especially, the developments of MIMO and NOMA are essential to achieving the first and third requirement, respectively. Furthermore, some researchers are interested in applying MIMO to NOMA in order to further enhance the throughput of NOMA. Although this is a natural idea to achieve between the first and third requirements, the complexity of signal processing should be reduced to satisfy the second requirement simultaneously. In addition, the energy consumption at each mobile device also has to be considered in traffic management of the smart city applications. Whereas, spatial modulation (SM) [6] has gained much attention as the MIMO technique which meets with the demand for spectral efficiency and energy efficiency [7]. In practical, the time-limited pulse shaping is crucial for considering the spectral efficiency of communication systems. Based on this fact, the bandwidth efficiencies of a classic MIMO system and SM have been compared in a fair manner, i.e., fair from the perspective of spectral efficiency, and the SM scheme using multiple RF chains has also been proposed [8]. Moreover, it has been demonstrated that the SM scheme is capable of outperforming the classic MIMO systems, under the assumptions of a low number of RF chains and realistic pulse shaping [8].

From these facts, we focus on utilizing SM for eMBB and mMTC services in this thesis, because of the following advantages of SM:

- **Low transmitter complexity**
  SM activates only a single antenna on data transmission, hence the transmitter only needs single RF-chain.
- **Low receiver complexity**
  The complexity of signal processing can be significantly reduced since inter-channel interference does not occur thanks to the simple transmission scheme of SM.
- **Spectral efficiency**
  With a low number of RF chains, SM can achieve high spectral efficiency like classic MIMO systems.

Although SM has the above advantages, there exist two crucial factors having an impact on the performance of SM. One is the spatial correlation of channels, and it degrades the performance of SM even if the receiver knows the perfect channel state information (CSI). Another is the accuracy of channel estimation, and it determines the accuracy of signal detection of SM as well as wireless communication systems. Furthermore, the channel estimation is a crucial task for multiuser communication systems.

Therefore, in this thesis, we study on a multiuser SM system and a coded SM system for mMTC and eMBB, respectively. These details are described and discussed in the later chapters.

1.3 Organization

We introduce the basics of SM and generalized SM (GSM) [9], e.g., system model and performance analysis, in chapter 2. Then, chapter 3 discusses how to estimate the channel state information for the uplink multiuser SM system. After we summarize the background to realize the highly-reliable SM and propose the optimization of SM with turbo trellis-coding in chapter 4, chapter 5 concludes our works.

Chapter 2

Spatial Modulation and Generalized Spatial Modulation

2.1 System Model

2.1.1 Transmission Scheme

The SM/GSM system is shown in Fig. 2.1. Let N_t and N_r denote the number of transmitting antennas (TAs) and receiving antennas (RAs), respectively. GSM utilizes N_a ($1 \leq N_a \leq N_t$) TAs to transmit the classic modulated signals [9], hence SM can be regarded as the special case of GSM with $N_a = 1$.

At each instance, $\mathbf{b} \in \{0,1\}^{B\times 1}$ is splitted into $\mathbf{b}_1 \in \{0,1\}^{B_1\times 1}$ and $\mathbf{b}_2 \in \{0,1\}^{B_2\times 1}$. After that, $\mathbf{b}_1$ and $\mathbf{b}_2$ are converted into a modulated symbol $s \in \mathcal{S}$ and a spatial vector $\mathbf{a} \in \mathbb{C}^{N_t\times 1}$, respectively. Here, $\mathcal{S}$ is the set of $M = 2^{B_1}$-ary modulated symbols, the N_a elements of $\mathbf{a}$ are one, and the others are zero. Finally, the signal $\mathbf{x} = s \cdot \mathbf{a} \in \mathbb{C}^{N_t\times 1}$ is transmitted. Here, we set $\mathbb{E}[|s|^2] = 1$ and $\|\mathbf{x}\|_2^2 = 1$ where $\mathbb{E}[\cdot]$ denotes the expected value.

Although the number of possible active antenna combinations is $\binom{N_t}{N_a}$, the number of combinations for transmission must be a power of two to make the bit mapping of antenna combinations a bijective. Therefore, only 2^{B_2} combinations can be used, where $B_2 = \lfloor \log_2 \binom{N_t}{N_a} \rfloor$, and $\lfloor\cdot\rfloor$ is the floor operation. The antenna combination is defined as $\ell = (\ell_1, \ell_2, \ldots, \ell_{N_a}) \in \Phi$, where ℓ_n indicates the index of n-th antenna in the ℓ, and Φ is the set of used antenna combinations.

In general, the transmission rates of SM/GSM systems are given by:

$$B = B_1 + B_2 = \log_2 M + \lfloor \log_2 N_t \rfloor, \text{ (SM)} \tag{2.1}$$

$$B = B_1 + B_2 = \log_2 M + \left\lfloor \log_2 \binom{N_t}{N_a} \right\rfloor, \text{ (GSM)}. \tag{2.2}$$

2.1.2 Channel Model

The channel matrix $\mathbf{H} \in \mathbb{C}^{N_r\times N_t}$ is modeled as below,

$$\mathbf{H} = \sqrt{\frac{K}{K+1}}\mathbf{H}_{\text{LOS}} + \sqrt{\frac{1}{K+1}}\mathbf{H}_0, \tag{2.3}$$

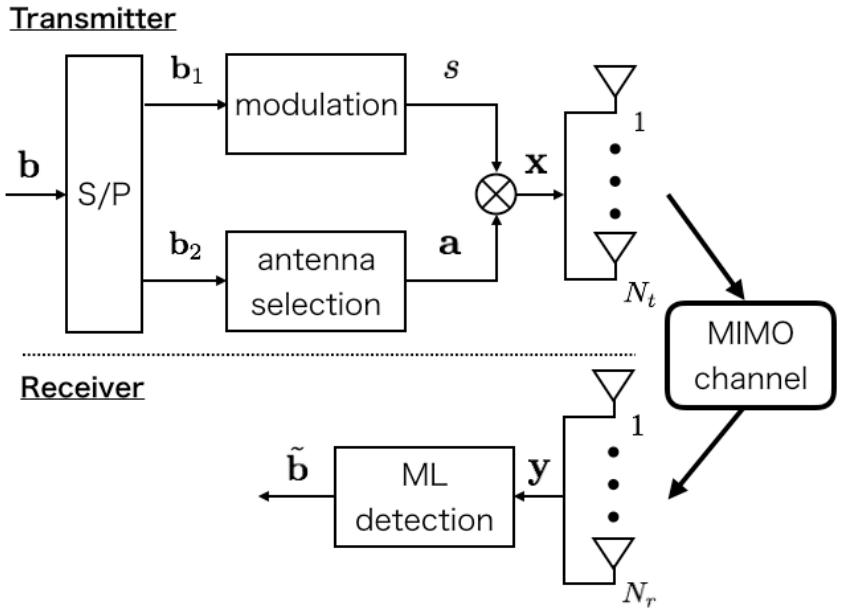

Figure 2.1: SM/GSM system model.

where $\sqrt{\frac{K}{K+1}}\mathbf{H}_{\text{LOS}}$ is the line-of-sight (LOS) component, $\sqrt{\frac{1}{K+1}}\mathbf{H}_0$ is the fading component, K is the Rician K-factor, $\mathbf{H}_{\text{LOS}}$ is a matrix with all elements being one, and $\mathbf{H}_0$ is a Rayleigh fading channel matrix whose components are the independent and identically distributed (i.i.d.) complex Gaussian random variables with zero-mean and unit-variance.

2.1.3 Detection

The received signal is represented as

$$\mathbf{y} = \mathbf{H}\mathbf{x} + \mathbf{z} \in \mathbb{C}^{N_r \times 1}, \tag{2.4}$$

where $\mathbf{z} \sim \mathcal{CN}(\mathbf{0}, \sigma_n^2 \mathbf{I}_{N_r})$ is an additive white Gaussian noise (AWGN) vector. At the receiver, the modulated symbol and the spatial vector are jointly decoded using the maximum likelihood (ML) detection, as follows,

$$[\hat{\ell}, \hat{s}] = \arg\max_{\ell, s} p_{\mathbf{y}}(\mathbf{y}|\mathbf{x}, \mathbf{H}). \tag{2.5}$$

The probability density function (PDF) of $\mathbf{y}$ given $\mathbf{x}$ and $\mathbf{H}$ is

$$p_{\mathbf{y}}(\mathbf{y}|\mathbf{x}, \mathbf{H}) = \frac{1}{(\pi\sigma_n^2)^{N_r}} \exp\left(-\frac{\|\mathbf{y} - \mathbf{H}\mathbf{x}\|_2^2}{\sigma_n^2}\right). \tag{2.6}$$

Therefore, the problem of (2.5) can be rewritten as:

$$[\hat{\ell}, \hat{s}] \quad = \quad \arg\min_{\ell, s} \sum_{i=1}^{N_r} |y_i - \mathbf{h}_i^{\text{r}} \mathbf{x}|^2, \tag{2.7}$$

where $\mathbf{h}_i^{\mathrm{r}} (\in \mathbb{C}^{1\times N_t})$ is the i-th row vector of $\mathbf{H}$. Finally, the estimate input bits $\hat{\mathbf{b}}$ are obtained from $\hat{\ell}$ and $\hat{s}$.

2.2 Optimal Set of Antenna Combinations

In this section, we review the optimal set of antenna combinations selection which has been introduced in [9]. The selection only performs in the case of Rayleigh channels, i.e., $K = 0$ in (2.3).

The bit error rate (BER) performance of GSM systems is determined by antenna combination, so that the optimal antenna combination set Φ_{opt} minimizes the average BER (ABER):

$$\Gamma_{\mathrm{opt}} = \arg\min_{\Gamma} \mathrm{ABER}, \tag{2.8}$$

where Γ is the set of parameters (N_t, N_a, Φ). In [9], the ABER is derived and given by

$$\mathrm{ABER} \leq \sum_{\ell,s} \sum_{\tilde{\ell},\tilde{s}} \frac{N(\mathbf{x}_{\ell,s}, \mathbf{x}_{\tilde{\ell},\tilde{s}}) I_{\frac{\sigma_n^2}{\sigma_n^2+\sigma^2_{D(\tilde{\ell},\tilde{s})}}}(N_r, N_r)}{2^{2B}}, \tag{2.9}$$

where we have the symbol $\mathbf{x}_{\ell,s}$ obtained by the signal s and the antenna combination ℓ, and $N(\mathbf{x}_{\ell,s}, \mathbf{x}_{\tilde{\ell},\tilde{s}})$ is the hamming distance between the bit sequences corresponding to $\mathbf{x}_{\ell,s}$ and $\mathbf{x}_{\tilde{\ell},\tilde{s}}$. Here, $I_x(a,b)$ is the regularized incomplete beta function given by

$$I_x(a,b) = \frac{1}{B(a,b)} \int_0^x t^{(a-1)}(1-t)^{(b-1)} dt, \tag{2.10}$$

with

$$B(a,b) = \int_0^1 t^{(a-1)}(1-t)^{(b-1)} dt. \tag{2.11}$$

Moreover, $\sigma^2_{D(\tilde{\ell},\tilde{s})}$ is given by

$$\sigma^2_{D(\tilde{\ell},\tilde{s})} = \sigma_n^2 + 2\Re\{s\tilde{s}^*\} d(\ell,\tilde{\ell}) + |s-\tilde{s}|^2 N_a, \tag{2.12}$$

where $\Re\{\cdot\}$ and $(\cdot)^*$ denote the real part of a complex number and the conjugate of a complex number, and $d(\ell,\tilde{\ell})$ is the number of elements where ℓ and $\tilde{\ell}$ differ from each other.

From (2.9), it can be noted that only $N(\mathbf{x}_{\ell,s}, \mathbf{x}_{\tilde{\ell},\tilde{s}})$ and $\sigma^2_{D(\tilde{\ell},\tilde{s})}$ depend on Γ. Moreover, it can be found that the following relation is satisfied:

$$I_{\frac{\sigma_n^2}{\sigma_n^2+\sigma^2_{D(\tilde{\ell},\tilde{s})}}}(N_r, N_r) \propto \frac{1}{\sigma^2_{D(\tilde{\ell},\tilde{s})}}. \tag{2.13}$$

Therefore, the optimization in (2.8) can be simplified to

$$\Gamma_{\mathrm{opt}} = \arg\min_{\Gamma} \sum_{\ell,s} \sum_{\tilde{\ell},\tilde{s}} \frac{N(\mathbf{x}_{\ell,s}, \mathbf{x}_{\tilde{\ell},\tilde{s}})}{\sigma^2_{D(\tilde{\ell},\tilde{s})}}. \tag{2.14}$$

2.3 Analyses of SM/GSM Performances

In this section, we review the analysis of SM/GSM performance from two viewpoints, i.e., ABER and achievable rate. We introduce the bound of the ABER of SM/GSM systems in Section 2.3.1, and the achievable rate, i.e., continuous-input continuous-output memoryless channel (CCMC) capacity and the descrete-input continuous-output memoryless channel (DCMC) capacity, in Section 2.3.2.

2.3.1 Average Bit Error Rate

The ABER in GSM has been often evaluated. Moreover, the analytical performance of GSM has been estimated using some bounds. In this section, we introduce the effective bound of ABER over Rayleigh channels, i.e., $K = 0$ in (2.3).

The ABER in GSM can be computed using the union bound technique, and can be expressed as follows,

$$\text{ABER} \leq \frac{1}{2^B} \sum_{\ell,s} \sum_{\tilde{\ell},\tilde{s}} \frac{N(\mathbf{x}_{\ell,s}, \mathbf{x}_{\tilde{\ell},\tilde{s}})}{B} \Pr\left(\mathbf{x}_{\ell,s} \to \mathbf{x}_{\tilde{\ell},\tilde{s}}\right), \tag{2.15}$$

where $\Pr(\mathbf{x}_{\ell,s} \to \mathbf{x}_{\tilde{\ell},\tilde{s}})$ is the probability of deciding on $\mathbf{x}_{\tilde{\ell},\tilde{s}}$ given that $\mathbf{x}_{\ell,s}$ is transmitted. The probability $\Pr(\mathbf{x}_{\ell,s} \to \mathbf{x}_{\tilde{\ell},\tilde{s}})$ is equal to the pairwise error probability (PEP) that $\mathbf{x}_{\tilde{\ell},\tilde{s}}$ is estimated when $\mathbf{x}_{\ell,s}$ is transmitted. Moreover, the PEP given $\mathbf{H}$ can be written as

$$\begin{aligned} & \Pr\left(\mathbf{x}_{\ell,s} \to \mathbf{x}_{\tilde{\ell},\tilde{s}} \middle| \mathbf{H}\right) \\ = \; & \Pr\left(\|\mathbf{y} - \mathbf{H}\mathbf{x}_{\ell,s}\|^2 > \|\mathbf{y} - \mathbf{H}\mathbf{x}_{\tilde{\ell},\tilde{s}}\|^2 \middle| \mathbf{H}\right) \\ = \; & \Pr\left(\sum_{i=1}^{N_r} |y_i - \mathbf{h}_i^{\mathrm{r}} \mathbf{x}_{\ell,s}|^2 > \sum_{i=1}^{N_r} |y_i - \mathbf{h}_i^{\mathrm{r}} \mathbf{x}_{\tilde{\ell},\tilde{s}}|^2 \middle| \mathbf{H}\right). \end{aligned} \tag{2.16}$$

Since, $\mathbf{x}_{\ell,s}$ is transmitted, $\mathbf{y} = \mathbf{H}\mathbf{x}_{\ell,s} + \mathbf{z}$, and $y_i = \mathbf{h}_i^{\mathrm{r}} \mathbf{x}_{\ell,s} + z_i$ $(i = 1, \ldots, N_r)$. Now, we can write

$$\begin{aligned} & \Pr\left(\mathbf{x}_{\ell,s} \to \mathbf{x}_{\tilde{\ell},\tilde{s}} \middle| \mathbf{H}\right) \\ = \; & \Pr\left(\sum_{i=1}^{N_r} |z_i|^2 > \sum_{i=1}^{N_r} |\mathbf{h}_i^{\mathrm{r}}(\mathbf{x}_{\ell,s} - \mathbf{x}_{\tilde{\ell},\tilde{s}}) + z_i|^2 \middle| \mathbf{H}\right) \\ = \; & \Pr\left(\sum_{i=1}^{N_r} 2\Re\{\mathbf{h}_i^{\mathrm{r}}(\mathbf{x}_{\tilde{\ell},\tilde{s}} - \mathbf{x}_{\ell,s}) z_i^*\} > \sum_{i=1}^{N_r} |\mathbf{h}_i^{\mathrm{r}}(\mathbf{x}_{\ell,s} - \mathbf{x}_{\tilde{\ell},\tilde{s}})|^2 \middle| \mathbf{H}\right), \end{aligned} \tag{2.17}$$

where $\sum_{i=1}^{N_r} 2\Re\{\mathbf{h}_i^{\mathrm{r}}(\mathbf{x}_{\tilde{\ell},\tilde{s}} - \mathbf{x}_{\ell,s})\}$ is a Gaussian random variable with mean zero and variance $2\sigma_n^2 \sum_{i=1}^{N_r} |\mathbf{h}_i^{\mathrm{r}}(\mathbf{x}_{\ell,s} - \mathbf{x}_{\tilde{\ell},\tilde{s}})|^2$. Therefore,

$$\Pr\left(\mathbf{x}_{\ell,s} \to \mathbf{x}_{\tilde{\ell},\tilde{s}} \middle| \mathbf{H}\right) = Q\left(\sqrt{\sum_{i=1}^{N_r} \frac{|\mathbf{h}_i^{\mathrm{r}}(\mathbf{x}_{\ell,s} - \mathbf{x}_{\tilde{\ell},\tilde{s}})|^2}{2\sigma_n^2}}\right), \tag{2.18}$$

where $Q(\cdot)$ denotes the Q-function. The argument in (2.18) is a central χ^2-distribution with $2N_r$ degrees of freedom. Computation of the unconditional PEP requires the expectation of the Q-function in (2.18) with respect to $\mathbf{H}$. The PEP can be obtained as follows [10]:

$$\begin{aligned} & \Pr\left(\mathbf{x}_{\ell,s} \to \mathbf{x}_{\tilde{\ell},\tilde{s}}\right) \\ = \; & \mathbb{E}_{\mathbf{H}}\left[\Pr\left(\mathbf{x}_{\ell,s} \to \mathbf{x}_{\tilde{\ell},\tilde{s}} | \mathbf{H}\right)\right] \\ = \; & \left(\frac{1-\mu(c)}{2}\right)^{N_r} \sum_{k=0}^{N_r-1} \binom{N_r-1-k}{k} \left(\frac{1+\mu(c)}{2}\right)^{k}, \end{aligned} \tag{2.19}$$

where $\mu(c) \triangleq \sqrt{\frac{c}{1+c}}$ and $c \triangleq \frac{1}{4\sigma_n^2} \sum_{i=0}^{N_r} |y_i - \mathbf{h}_i^{\mathrm{r}}(\mathbf{x}_{\ell,s} - \mathbf{x}_{\tilde{\ell},\tilde{s}})|^2$.

2.3.2 CCMC and DCMC Capacity

The classic CCMC capacity C_{CCMC} is given by

$$C_{\mathrm{CCMC}} = \mathbb{E}_{\mathbf{H}}\left[\sum_{i=1}^{\mathrm{rank}(\mathbf{Q})} \log_2\left(1 + \frac{\rho}{N_t}\lambda_i\right)\right] \text{ [bits/s/Hz]}, \tag{2.20}$$

where we have

$$\mathbf{Q} = \begin{cases} \mathbf{H}\mathbf{H}^{\mathrm{H}} & (N_r < N_t) \\ \mathbf{H}^{\mathrm{H}}\mathbf{H} & (N_r \geq N_t) \end{cases}. \tag{2.21}$$

Here, ρ is the signal-to-noise ratio (SNR), λ_i is the ith eigenvalue of $\mathbf{Q}$, and $[\cdot]^{\mathrm{H}}$ denotes the Hermitian transpose of a vector and a matrix. CCMC capacity is derived under the assumption that the input signals follow the complex Gaussian distribution. Furthermore, CCMC capacity becomes the theoretical upper bound of the average mutual information (AMI).

The DCMC capacity C_{DCMC} is given by [11]:

$$C_{\mathrm{DCMC}} = B - \frac{1}{2^B}\sum_{\ell,s} \mathbb{E}_{\mathbf{H},\mathbf{z}}\left[\log_2 \sum_{\tilde{\ell},\tilde{s}} e^{\eta[\ell,s,\tilde{\ell},\tilde{s}]}\right] \text{ [bits/s/Hz]}, \tag{2.22}$$

where $\mathbb{E}_{\mathbf{H},\mathbf{z}}[\cdot]$ denotes the expectation with respect to $\mathbf{H}$ and $\mathbf{z}$, and we have

$$\eta[\ell, s, \hat{\ell}, \hat{s}] = \frac{-\|\mathbf{H}(\mathbf{x}_{\ell,s} - \mathbf{x}_{\tilde{\ell},\tilde{s}}) + \mathbf{z}\|^2 + \|\mathbf{z}\|^2}{\sigma_n^2}. \tag{2.23}$$

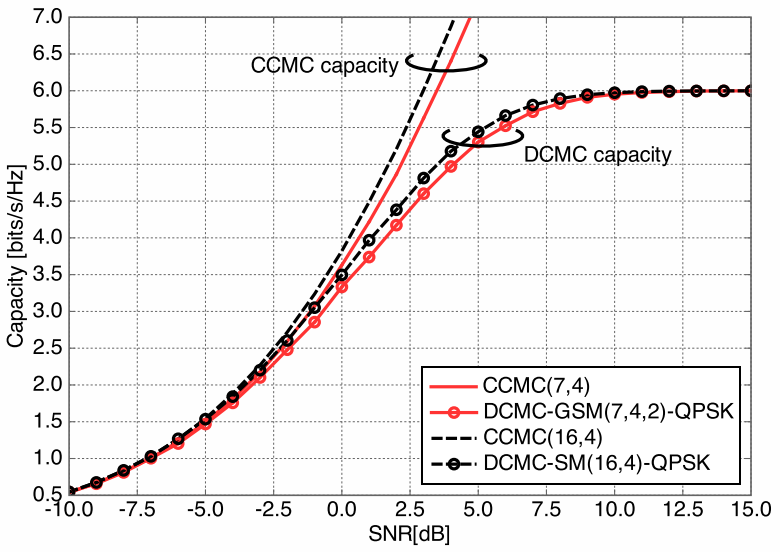

Figure 2.2: CCMC capacity and DCMC capacity comparison between GSM and SM over Rayleigh channels. Red solid lines denote CCMC capacity and DCMC capacity where $N_t = 7$. Black dashed lines denote CCMC capacity and DCMC capacity where $N_t = 16$.

2.4 Numerical Results

In this section, we provide the results of uncoded GSM performance in term of capacity and BER where $N_r = 4$. We also use the quadrature phase shift keying (QPSK) symbols as the modulated symbols. Note that the parameters of GSM and SM are expressed as GSM(N_t, N_r, N_a) and SM(N_t, N_r).

2.4.1 Capacity Comparison

To confirm the effect of GSM, GSM(7,4,2) and SM(16,4) with QPSK, where the transmission rates of both systems are 6 [bits/s/Hz], are evaluated. Figure 2.2 shows the CCMC capacities with N_t =7 and 16 respectively and the DCMC capacity of GSM(7,4,2) and SM(16,4) with QPSK over Rayleigh channels ($K = 0$). The result indicates that both theoretical and actual AMI of SM systems outperforms those of GSM systems because of the superiority of the number of TAs. However, the gap of DCMC capacities between GSM and SM is slight and GSM needs only about half TAs of SM. Therefore, the results also imply that GSM can achieve a target transmission rate with fewer TAs than SM.

2.4.2 BER Performance

Figure 2.3 shows the bit error rate (BER) performance of GSM and SM over Rayleigh channels ($K = 0$). The result shows that the BER performance of GSM(7,4,2) is almost the same as that of SM(16,4). Although the performance of GSM is slightly worse than that of SM, this is a predictable result from Fig. 2.2.

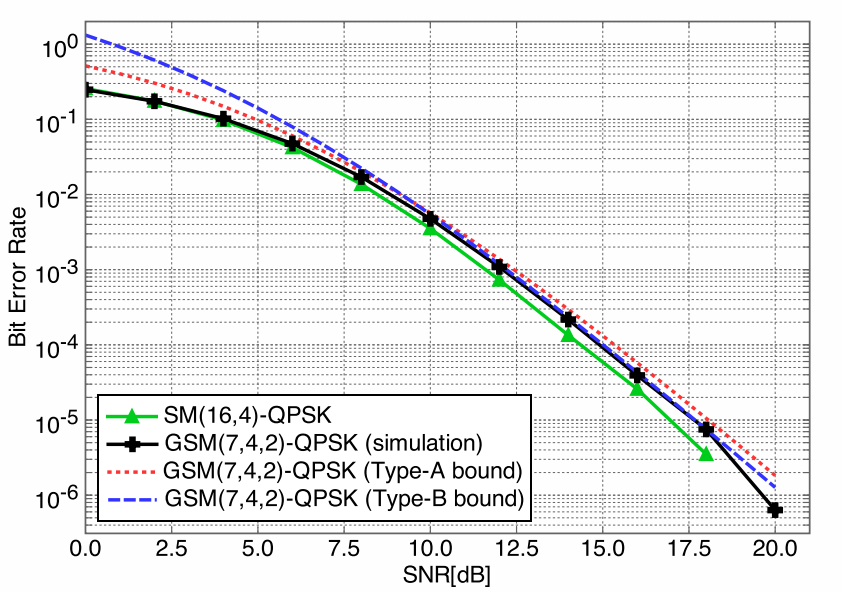

Figure 2.3: BER comparison between GSM and SM over Rayleigh channels where transmission rate is 6 [bits/s/Hz]. Dotted line denotes Type-A bound given by (2.9) and dashed line denotes Type-B bound given by (2.15).

Moreover, we evaluate two bounds shown in Fig. 2.3. Note that Type-A bound is given by (2.9) and Type-B bound is given by (2.15). Figure 2.3 indicates that Type-B bound give the tighter upper bound than Type-A bound. Hence, Type-B bound can be a sufficiently effective metric to design GSM systems.

Figure 2.4 shows the BER performance of GSM and SM over Rayleigh channels and Rician channels with $K = 3$. Here, the transmission rate is 5 [bits/s/Hz]. The result indicates that the gap of BER performances of GSM and SM in Rician channels is larger since the antenna combinations in GSM are chosen to minimize ABER over Rayleigh channels.

Hence, over Rician channels, the effect of channel correlations should be considered to decide the combinations.

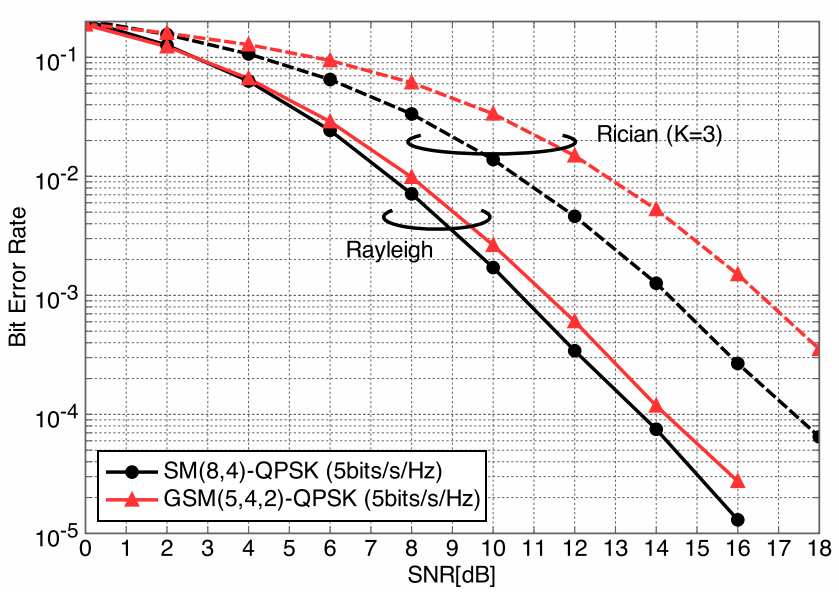

Figure 2.4: BER comparison between GSM and SM over Rayleigh and Rician (K=3) channels where the transmission rate is 5 [bits/s/Hz].

2.5 Chapter Summary

In this chapter, we introduced the fundamental of SM and GSM systems and reviewed their performances, such as capacity and ABER. The analysis of Section 2.3.1 estimates the BER performance, while the AMI analyses of Section 2.3.2 provide the theoretical upper bound and the upper bound for the system using the discrete-input signals. We also observed the fundamental performances of SM and GSM via computer simulations.

In the following chapters, we consider the system for multiuser scenarios and the coded system. We approach the uncoded multiuser SM system in the next chapter.

Chapter 3

Channel Estimation for Multiuser Spatial Modulation

3.1 Background

As introduced in Chapter 1, the development of multiple access schemes is crucial to satisfying the requirements of mMTC services. On one hand, reference [12] reported that a multiuser SM system outperforms the multiuser MIMO system where the base station (BS) has multiple antennas while all user equipments (UEs) have a single antenna. Therefore, multiuser detection (MUD) for multiuser SM system has been studied in some literature [13, 14]. Furthermore, the combination of SM/GSM and NOMA has also been investigated [15, 16], since the movement to standardize NOMA has been active [17].

Most of MUD for multiuser SM utilize compressed sensing to make use of the characteristics of the transmitted signal, which has only one non-zero element and can be regarded as a sparse signal. However, these detections, e.g., references [13, 16], have been discussed under the impractical assumption, i.e., BS knows the perfect channel state information. In practice, the accuracy of signal detection in MIMO systems depends on that of the estimation of channel information. Therefore, we study the channel estimation for multiuser SM system.

The channel estimation problem, where BS has multiple antennas, can be regarded as a multiple measurement vector-compressed sensing (MMV-CS). Moreover, MMV-CS can be transferred to a block-sparse single measurement vector-CS (BS-SMV-CS) [18]. Based on the above idea, we formulate the channel estimation problem as BS-SMV-CS and propose the reconstruction algorithm based on complex approximate message passing (CAMP) [19] to solve the BS-SMV-CS efficiently. Furthermore, we consider the multiuser SM system where a few users are active and transmit data to BS by following time-division multiple access (TDMA). In this chapter, we evaluate the performances of the above system via computer simulations.

3.2 System Model

Figure 3.1 shows the multiuser SM system where BS with N_r antennas and U UEs with N_t antennas and $N_a (P = N_t/N_a \in \mathbb{N})$ RF-chains exist. The uplink transmission, where $S (S < U)$ UEs are randomly activated to transmit data to BS, is assumed in this chapter.

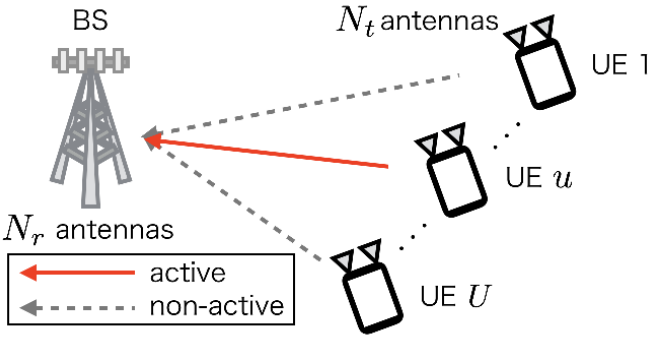

Figure 3.1: The multiuser SM system.

3.2.1 Training Phase

Each UE has N_a unique pilot sequences, then let $\mathbf{a}_i \in \mathbb{C}^{L\times 1}$ denote the pilot sequences for $i = 1, 2, \ldots, UN_a$. Moreover, each pilot sequence $\mathbf{a}_i$ satisfies that $\|\mathbf{a}_i\|_2 = 1$, and the set of indices of pilot sequences of UE u is defined as $\mathcal{A}_u \triangleq \{(u-1)N_a + 1, (u-1)N_a + 2, \ldots, uN_a\}$.

In the training phase, S active UEs transmit P times own unique sequences to BS like Fig. 3.2. In this chapter, the channel estimation for the multiuser SM system is described focusing on only one pilot transmission, thus BS receives the signal in the training phase:

$$\begin{aligned}\mathbf{Y} &= \sum_{u\in\{1,2,\ldots,U\}} \alpha_u \sum_{i\in\mathcal{A}_u} \mathbf{a}_i \mathbf{h}_i^{\mathrm{T}} + \mathbf{Z} \in \mathbb{C}^{L\times N_r} \\ &= \sum_{u\in\mathcal{U}} \sum_{i\in\mathcal{A}_u} \mathbf{a}_i \mathbf{h}_i^{\mathrm{T}} + \mathbf{Z} \in \mathbb{C}^{L\times N_r},\end{aligned} \tag{3.1}$$

where $\mathcal{U}$ is the set of active users, α_u is the indicator following:

$$\alpha_u = \begin{cases} 1 & (u \in \mathcal{U}) \\ 0 & (\text{otherwise}) \end{cases}, \tag{3.2}$$

each row of $\mathbf{Z}$ is the AWGN vector following $\mathcal{CN}(\mathbf{0}, \sigma_n^2 \mathbf{I}_{N_r})$, and $\mathbf{h}_i \sim \mathcal{CN}(\mathbf{0}, \mathbf{I}_{N_r})$ is the vector having N_r channel coefficients between the ith antenna and BS. Here, $[\cdot]^{\mathrm{T}}$ denotes the transpose of a vector and a matrix.

3.2.2 Problem Formulation for Channel Estimation

For $i \in \mathcal{A}_u$, we set $\mathbf{x}_i = \alpha_u \mathbf{h}_i \in \mathbb{C}^{N_r\times 1}$, then (3.1) can be written as:

$$\mathbf{Y} = \mathbf{A}\mathbf{X} + \mathbf{Z} \in \mathbb{C}^{L\times N_r}, \tag{3.3}$$

where $\mathbf{Y} = [\mathbf{y}_1, \ldots, \mathbf{y}_{N_r}] \in \mathbb{C}^{L\times N_r}$, $\mathbf{A} = [\mathbf{a}_1, \ldots, \mathbf{a}_{UN_a}] \in \mathbb{C}^{L\times UN_a}$, and $\mathbf{X} = [\mathbf{x}_1, \ldots, \mathbf{x}_{UN_a}]^{\mathrm{T}} \in \mathbb{C}^{UN_a\times N_r}$.

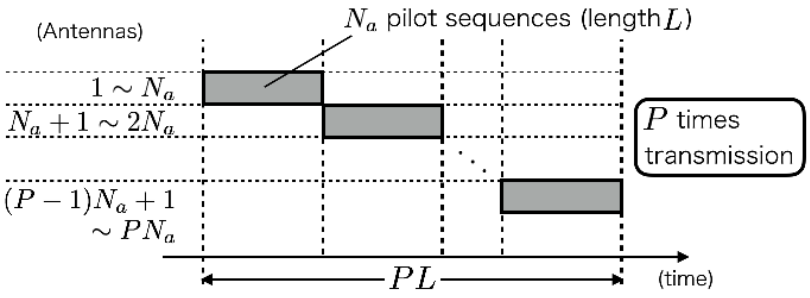

Figure 3.2: The example of the processing of the active UE in the traning phase.

Furthermore, by using a Kronecker product $\otimes$, (3.3) can be expressed as:

$$\mathbf{y} = (\mathbf{A} \otimes \mathbf{I}_{N_r})\mathbf{x} + \mathbf{z} = \mathbf{D}\mathbf{x} + \mathbf{z} \in \mathbb{C}^{LN_r \times 1}, \tag{3.4}$$

where we have $\mathbf{y} = [\mathbf{y}_1; \ldots; \mathbf{y}_{N_r}] \in \mathbb{C}^{LN_r \times 1}$, $\mathbf{x} = [\mathbf{x}_1; \ldots; \mathbf{x}_{UN_a}] \in \mathbb{C}^{UN_aN_r \times 1}$, and $\mathbf{D} = [\mathbf{D}[1], \ldots, \mathbf{D}[UN_a]] \in \mathbb{C}^{LN_r \times UN_aN_r}$, $(\mathbf{D}[u] \in \mathbb{C}^{LN_r \times N_r})$. The channel estimation can be regarded as the BS-SMV-CS with SN_a block-sparse signal, since $\mathbf{x}$ can be regarded as the vector having UN_a subvectors with length N_r. Therefore, we apply the algorithm proposed in the following section to the BS-SMV-CS of (3.4).

3.2.3 Data Transmission Phase

After the channel training phase, active UEs transmit data with spreading to a time domain by own pilot sequence. Let $\mathcal{U}_{\text{est}}$ and T denote the set of UEs regarded as an active UE by BS and the duration for channel estimation and data transmission, respectively. The set $\mathcal{U}_{\text{est}}$ consists of the indices satsfying

$$\sum_{\ell=1}^{N_t} \|\hat{\mathbf{h}}_u^{(\ell)}\|_2 \geq N_t \sqrt{N_r \sigma_n^2} \tag{3.5}$$

where $\hat{\mathbf{h}}_u^{(\ell)}$ is the estimated channel between the ℓ th antenna of UE u and BS. Since the length of pilot sequence is L, the number of the transmitted SM symbols for the duration T is

$$T_{\text{data}} = \left\lfloor \frac{T - PL}{L} \right\rfloor \text{ [symbols]}. \tag{3.6}$$

BS despreads the received signals by the pilot sequences corresponding to $\mathcal{U}_{\text{est}}$. After then, BS estimates the transmitted symbols by ML detection.

The effective throughput of this system is defined as:

$$R_{\text{system}} \triangleq T_{\text{data}} \cdot \left(\left\lfloor \log_2 \binom{N_t}{N_a} \right\rfloor + \log_2 Q \right) \sum_{u \in \{\mathcal{U} \cap \mathcal{U}_{\text{est}}\}} (1 - P_e^{(u)}) \text{ [bits]} \tag{3.7}$$

Algorithm 1 BS-CAMP

Require: $\mathbf{y} \in \mathbb{C}^{LN_r \times 1}$ (The measurement vector)
$\mathbf{D} \in \mathbb{C}^{LN_r \times UN_aN_r}$ (The measurement matrix)
$\tau \in \mathbb{R}$ (The parameter to determine the threshold in (3.9))
$t_{\max} \in \mathbb{N}$ (The maximum number of iterations)
Ensure: $\hat{\mathbf{x}} \in \mathbb{C}^{UN_aN_r \times 1}$ (The estimate of $\mathbf{x}$)
1: Initialization: $\bar{\mathbf{x}}^0 = \mathbf{0}, \mathbf{z}^0 = \mathbf{y}$
2: **for** $t = 1$ to $t_{\max}$ **do**
3: $\quad \tilde{\mathbf{x}}^t = \mathbf{D}^{\mathrm{H}}\mathbf{z}^{t-1} + \bar{\mathbf{x}}^{t-1}$
4: $\quad$ Calculate σ_t by (3.10)
5: $\quad \bar{\mathbf{x}}^t = \eta^{\mathrm{bsoft}}(\tilde{\mathbf{x}}^t; \tau\sigma_t)$
6: $\quad \mathbf{z}^t = \mathbf{y} - \mathbf{D}\bar{\mathbf{x}}^t + b_t\mathbf{z}^{t-1}$
7: **end for**
8: **return** $\hat{\mathbf{x}} = \bar{\mathbf{x}}^{t_{\max}}$

where Q denotes the number of the modulated symbols and $P_e^{(u)}$ is the frame-error probability that the symbols transmitted by UE u during $T - L$ are detected incorrectly. Moreover, the effective throughput of (3.7) is bounded by the performance where $\mathcal{U}_{\mathrm{est}} = \mathcal{U}$ and $P_e^{(u)} = 0$ for all u:

$$R_{\mathrm{system}} \leq S \cdot T_{\mathrm{data}} \cdot \left(\left\lfloor \log_2 \binom{N_t}{N_a} \right\rfloor + \log_2 Q \right). \tag{3.8}$$

3.3 Block-Sparse Complex Approximate Message Passing

We propose the *block-sparse complex approximate message passing* (BS-CAMP) for the channel estimation. BS-CAMP is an algorithm which applies the function [20] given by:

$$\begin{aligned} \eta^{\mathrm{bsoft}}(\mathbf{u}; \lambda_{\mathrm{th}}) &\triangleq (\eta(\mathbf{u}_1; \lambda_{\mathrm{th}}), \ldots, \eta(\mathbf{u}_{KN_a}; \lambda_{\mathrm{th}})), \\ \eta(\mathbf{u}_i; \lambda_{\mathrm{th}}) &\triangleq \max\left\{ \|\mathbf{u}_i\|_2 - \lambda_{\mathrm{th}}, 0 \right\} \frac{\mathbf{u}_i}{\|\mathbf{u}_i\|_2}, \quad \mathbf{u}_i \in \mathbb{C}^{N_r \times 1}, \end{aligned} \tag{3.9}$$

to CAMP[19]. Here, λ_{th} in (3.9) is the threshold of ℓ_2-norm of $\mathbf{u}_i$.

The algorithm of BS-CAMP is shown in Algorithm 1. In BS-CAMP, the threshold in (3.9) is determined by two parameters τ and σ_t, i.e., $\lambda_{\mathrm{th}} = \tau\sigma_t$. In this work, we set $\tau = \sqrt{N_r}$ and update σ_t by [19]:

$$\sigma_t = \sqrt{\frac{1}{\ln 2}} \mathrm{median}(|\tilde{\mathbf{x}}^t|), \tag{3.10}$$

where $|\tilde{\mathbf{x}}^t|$ is the vector whose elements are the absolute value of elements of $\tilde{\mathbf{x}}^t$ and median($\mathbf{v}$) is the function returning the median of the elements of $\mathbf{v}$. Moreover, the parameter b_t to update

Table 3.1: Simulation parameters.

–	BS-CAMP	BOMP
U	60	
S	6	
N_t	4	
N_a	1	
L	20	
Number of Iterations	30	–

the residual $\mathbf{z}^t$ is calculated by:

$$\begin{aligned} b_t &\equiv \frac{1}{2LN_r}\text{div } \eta^{\text{bsoft}}(\tilde{\mathbf{x}};\tau\sigma_t)\Big|_{\tilde{\mathbf{x}}=\tilde{\mathbf{x}}^t} \\ &= \frac{1}{2LN_r}\sum_{i=1}^{KN_a}\left(2N_r-(2N_r-1)\frac{\tau\sigma_t}{\|\tilde{\mathbf{x}}_i^t\|_2}\right)\left(\max\left\{\|\tilde{\mathbf{x}}_i^t\|_2-\tau\sigma_t,0\right\}\right). \end{aligned} \tag{3.11}$$

3.4 Numerical Results

In this section, we investigate the accuracy of the channel estimation by the proposed algorithm and the effect of the accuracy on the effective throughput of the multiuser SM system. Hence, the normalized mean squared error (NMSE) performance of the channel estimation and the effective throughput are evaluated via computer simulations. The fixed simulation parameters are shown in Table 3.1. For all simulations, the pilot sequences $\mathbf{A}$ are obtained from the design based on cyclic group [21]. Moreover, let $\text{SNR}_{\text{pilot}}$ and SNR_{sig} denote the SNR in the training phase and the data transmission phase, respectively.

3.4.1 NMSE Performance

The NMSE performances of the channel estimation, where $L = 20$ and $S = 6$, are shown in Fig. 3.3, which includes the performances of block orthogonal matching pursuit (BOMP) [22]. Note that BOMP has to know the number of active UEs S as a priori information, however, BS-CAMP does not need to know S.

Figure 3.3 indicates that BS-CAMP is inferior to BOMP in SNR higher than 10 dB, since the setup of BS-SMV-CS with $N_a = 1$, i.e., the columns of $\mathbf{D}[u]$ are orthonormal for each u, in fact, it is a sufficient condition for perfect recovery using BOMP under the noise-free case [22]. From the result and the fact that BS-CAMP does not need to know S, BS-CAMP has the potential to further improve the accuracy of channel estimation and the capability to support more UEs thanks to its advantage and performance.

3.4.2 Effective Throughput Performance

The effective throughput defined as (3.7) is evaluated and the result is shown in Fig. 3.4, where $S = 6$, $T = 1,000$, and $\text{SNR}_{\text{pilot}} = 15$[dB]. According to Fig. 3.4, when N_r is smaller, the gap

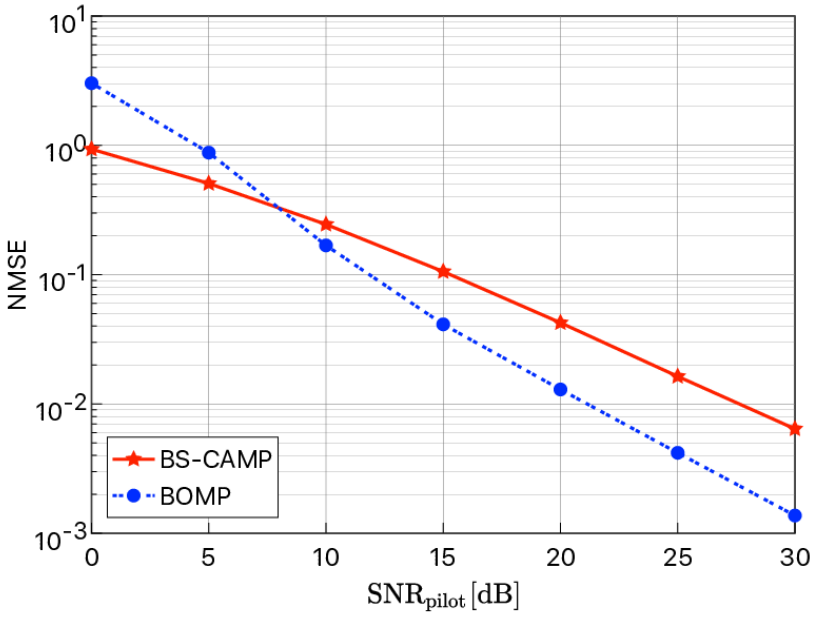

Figure 3.3: The NMSE performances of the channel estimation by BS-CAMP and BOMP, where $L = 20$ and $S = 6$.

between the ideal and actual performances becomes larger. This is a natural result, however, it is noteworthy that even the "ideal" performance achieves about 70% of the maximum value where $N_r = 4$. This is caused by the degradation of the performance of multiuser detection because of the relation of $N_r \geq N_t$. Moreover, the performance gaps decrease with the increase of N_r, and both BS-CAMP and BOMP performances can almost achieve the maximum value. In particular, the gap between BS-CAMP and BOMP becomes slight, hence, the channel estimation using BS-CAMP can be practical in the multiuser SM system from the aspect of the characteristic of the algorithm which does not need the number of active UEs.

3.5 Chapter Summary

In this chapter, for multiuser SM systems, we have proposed BS-CAMP algorithm for the channel estimation. After we described the formulation of the channel estimation, the simple multiuser SM system is assumed to investigate the effect of the proposed algorithm. Finally, we evaluated the performances of the proposed method via computer simulations from two aspects: the accuracy of the channel estimation and the effect of the reduction of the overhead. Then, these results suggested that BS-CAMP is practical for the multiuser SM system.

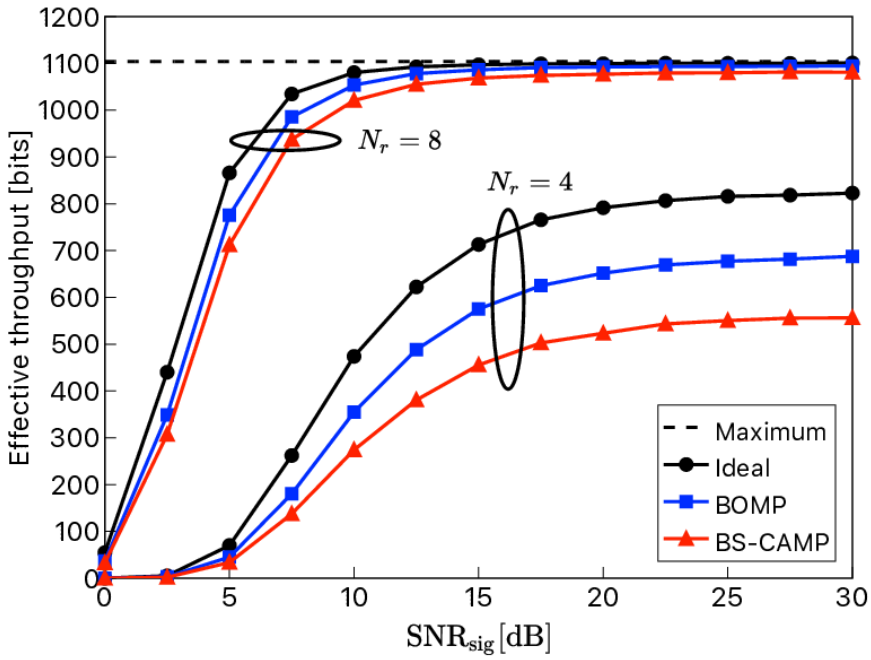

Figure 3.4: The effective throughput comparison versus $\mathrm{SNR}_{\mathrm{sig}}$ where $S = 6$, $T = 1,000$, and $\mathrm{SNR}_{\mathrm{pilot}} = 15$[dB]. The block dot line shows the maximum value of the effective throughput. The black solid lines are labeled as "ideal" and shows the results which are achieved where BS knows the channel state information and active UEs perfectly. The red lines are the results of BS-CAMP, while the blue lines are the results of BOMP.

Chapter 4

Optimization of Turbo-Trellis Coded Spatial Modulation

4.1 Background

In SM, the attainable transmission rates can be increased, even though the transmitter and receiver complexity is considerably reduced [6]. However, its performance degrades for transmission over spatially correlated (SC) channels, since the channel coefficients become close values mutually. Hence, the effect of correlation should be considered. As a promising technique of reducing the effect of correlation, coded spatial modulation (CSM) has been proposed [23, 24, 25, 26, 27] for mitigating the decision errors imposed by the reduced Euclidean distance that was inflicted by the antenna correlation. Of course, since the error-correcting code is essential to improve throughput performance, CSM also has the potential to achieve the requirements introduced in Chapter 1.

To elaborate, in trellis coded spatial modulation (TCSM)[23], the Euclidean distance within a specific symbol subset was maximized by following the principles of classic trellis coded modulation (TCM) [28]. However, the coding gain of large classic constellation sets was reduced, since a gradually increased number of bits remained uncoded, as the code-rate was increased from R=2/3 to 3/4, 4/5, etc. In order to further improve the performance of CSM, a new scheme termed as SM with trellis-coding (SM-TC) has been proposed in [24], where all information bits are channel-encoded. However, the improved performance of SM-TC over that of TCSM was attained at an increased decoding complexity, which escalated exponentially upon increasing the number of bits/channel use (bpcu).

To deal with this impediment, a bit-interleaved coded spatial modulation (BICSM) scheme has been proposed [25], which is based on classic bit-interleaved coded modulation (BICM) [29]. In the scheme, the information bits are mapped both onto the TA indices and to data symbols after the bits are fed into channel encoder and bit-interleaver. Although BICSM is robust both against i.i.d. fading and SC channels, its performance is suboptimal since the channels become independent in bit level. In order to further improve its performance, the iterative decoding and demapping have to be invoked.

As a further advance, turbo trellis-coded spatial modulation (TTCSM) has been proposed [26], which inherits its philosophy from turbo trellis-coded spatial modulation (TTCM) [30],

and its design is similar to that of TCSM [23]. Thanks to iterative decoding, the coding gain of TTCSM is 2 dB higher than that of TCSM [23]. In an attempt to increase the coding gain, spatial modulation with turbo trellis coding (SM-TTC) has also been proposed [27], where all information bits are encoded by the same encoder as in the TTCSM scheme of [26].

However, the optimization of the channel code conceived for CSM schemes based on TTCM has not been directly motivated by attaining near-capacity performance. One of the associated challenges is that the full search of all legitimate generator polynomials (GPs) becomes excessive for a high number of bpcu. The specific code search algorithm, which finds the best code for TTCM using symbol-based extrinsic information transfer (EXIT) charts [31] has been proposed in [32]. The GP search algorithm can simply find the best code for TTCM by finding the GP, which results in an open EXIT-tunnel at the lowest SNR. However, the computational complexity of evaluating all GPs at a high number of bpcu is still high.

Hence, in this chapter, we propose a low-complexity code search method for CSM scheme based on TTCM, specifically focusing on SM-TTC. To reduce the computational complexity of code search, our method exploits the area property of symbol-based EXIT charts instead of the EXIT trajectory, and it enables us to find the best GP without executing iterative decoding, whilst the code search algorithm of [32] relies on it. Moreover, in order to further simplify our GP search, we introduce a relaxation, which allows us to conceive a low-complexity capable of determining the approximate performance limit of SM-TTC without evaluating the EXIT trajectory.

4.2 System Model of SM-TTC

4.2.1 Transmitter

We consider a SM-TTC system with N_t TA elements and N_r RA elements as illustrated in Fig. 4.1. We assume that the number of TA elements is an integer power of 2, i.e., $N_t = 2^{n_a}$, and the transmitter employs M-ary digital modulation, where $M = 2^{n_s}$. Let $\mathcal{S}$ denote the set of modulated symbols. Note that the bandwidth efficiency of the classic SM system is $R^{(\mathrm{SM})} = n_a + n_s = \log_2(N_t M)$ bpcu.

At any moment t, the transmitter processes a bit sequence $\mathbf{u}(t) = [u_1, \ldots, u_k]$ ($u_i \in \{0, 1\}$, for $i = 1, \ldots, k$). Each sequence $\mathbf{u}(t)$ is fed into a parallel-concatenated convolutional encoder, which uses a symbol-based interleaver. The two component encoders in Fig. 4.1 are identical recursive systematic convolutional (RSC) encoders of rate $k/(k+1)$. Therefore, k satisfies $k + 1 = R^{(\mathrm{SM})}$. In addition, the symbol-based interleaver denoted by π in Fig. 4.1 treats a k-bit input string as one symbol and maps the odd (even) indexed symbols to another odd (even) position, using the odd-even separation (OES) interleaver of [30]. The sequence at the output of RSC encoder1 in Fig. 4.1 is denoted by $\mathbf{v}_1(t) = [\mathbf{u}(t), c_p^{(1)}]$, where $c_p^{(1)} \in \{0, 1\}$ is the $(k+1)$-st bit of $\mathbf{v}_1(t)$ and the parity bit generated from $\mathbf{u}(t)$ by RSC Encoder1. On the other hand, the output of RSC Encoder2 in Fig. 4.1 is deinterleaved using the deinterleaver, which is denoted by π^{-1} in Fig. 4.1 and performs the inverse operation of π. The resultant sequence is denoted by $\mathbf{v}_2(t) = [\mathbf{u}(t), c_p^{(2)}]$, where $c_p^{(2)} \in \{0, 1\}$ is the $(k+1)$-st bit of $\mathbf{v}_2(t)$ and the parity bit generated from $\mathbf{u}(t)$ by RSC encoder2. The output of the channel encoder is denoted by $\mathbf{v}(t) = [\mathbf{u}(t), c(t)]$, where $c(t) \in \{0, 1\}$ is $c_p^{(1)}$ when the index t is even, otherwise, $c_p^{(2)}$. Finally,

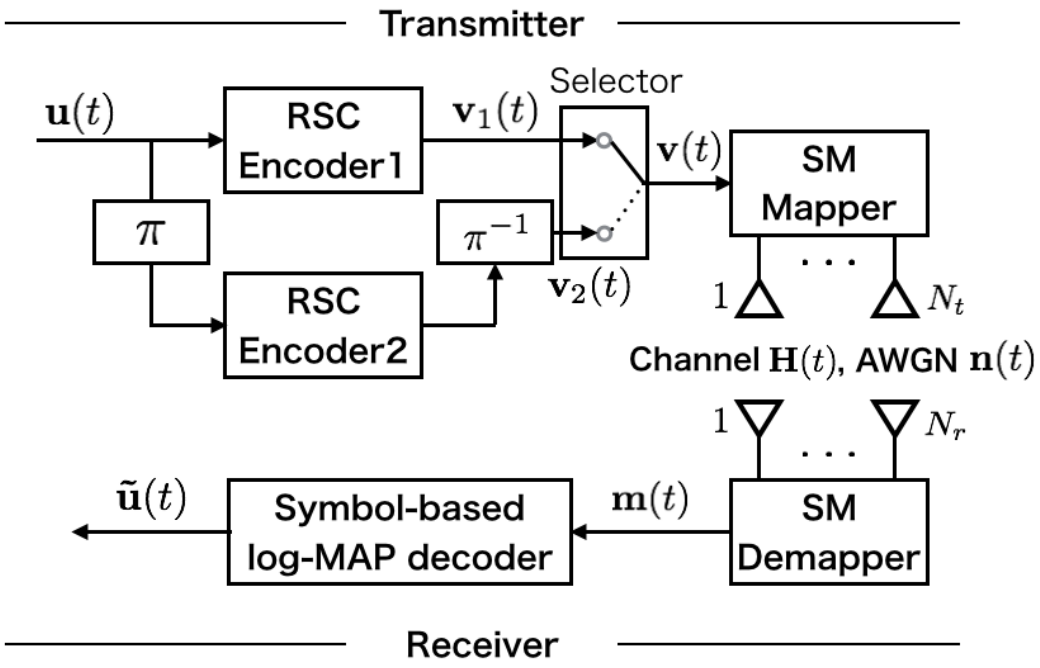

Figure 4.1: Transceiver structure of SM-TTC system.

the SM mapper determines the activated TA index and the modulated symbol using $\mathbf{v}(t)$. The n_s-bit sequence $[v_1, \ldots, v_{n_s}]$ and the n_a-bit sequence $[v_{n_s+1}, \ldots, v_{n_s+n_a}]$ are mapped to the data symbol and the antenna index, respectively. Here, the labeling of both data symbol and antenna index are natural labeling.

The transmitted signal is $\mathbf{x}(t) = [x_1, \ldots, x_i, \ldots, x_{N_t}]^{\mathrm{T}}$, where $x_i \in \{\mathcal{S} \cup \{0\}\}$.Note that if the m-th antenna is selected, then $x_i = 0$ for all $i \neq m$. In other words, the position of the non-zero element denotes the TA index and its value indicates the transmitted symbol. We assume a power constraint of unity, i.e., $\mathbb{E}[\mathbf{x}^{\mathrm{H}}(t)\mathbf{x}(t)] = 1$.

4.2.2 Channel Model

A MIMO channel is denoted by an $N_r \times N_t$ matrix $\mathbf{H}(t)$. In this paper, we consider two different MIMO channels. One of the channel models is a Rayleigh fading channel, which is spatially uncorrelated. The MIMO channel matrix is modeled by the matrix $\breve{\mathbf{H}}(t)$, i.e., $\mathbf{H}(t) = \breve{\mathbf{H}}(t)$. The i-th row and j-th column element of $\breve{\mathbf{H}}(t)$ is denoted by $\breve{h}_{ij}$, which is an i.i.d. complex Gaussian random variable with zero mean and unit variance. The another channel model is an SC MIMO channel. Employing the Kronecker model, the SC MIMO channel can be modeled as [33]:

$$\mathbf{H}(t) = \Sigma_{\mathrm{rx}}^{\frac{1}{2}} \breve{\mathbf{H}}(t) \left(\Sigma_{\mathrm{tx}}^{\frac{1}{2}} \right)^{\mathrm{H}}, \tag{4.1}$$

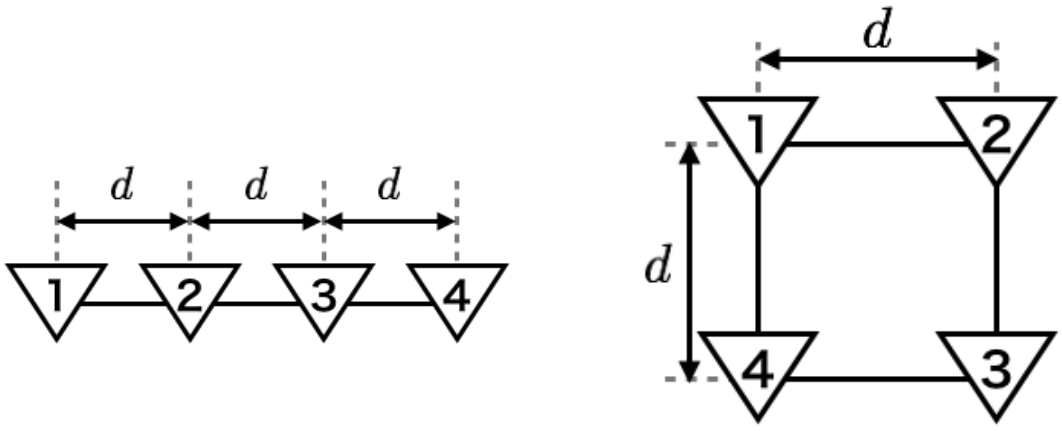

(a) A linear antenna array

(b) A square antenna array

Figure 4.2: Geometrical models of two antenna arrays.

where $\Sigma_{\text{tx}} \in \mathbb{C}^{N_t \times N_t}$ and $\Sigma_{\text{rx}} \in \mathbb{C}^{N_r \times N_r}$ are the Hermitian symmetric transmitter and receiver correlation matrices, respectively. In this paper, we consider two different antenna arrays. One arrangement of antenna array is a linear antenna array at the transmitter and the receiver, where all antenna elements are arranged on a straight line at equal intervals d. This model of the antenna array is shown in Fig. 4.2(a). Then, it is assumed that the transmitter and receiver correlation matrices obey the exponential correlation model of [34], and their entries are defined as

$$[\Sigma_X]_{p,q} = \begin{cases} \gamma^{q-p}, & p \leq q \\ ([\Sigma_X]_{q,p})^* & p > q \end{cases}, \quad X \in \{\text{tx}, \text{rx}\}, \tag{4.2}$$

where γ is a fixed correlation coefficient between the adjacent antenna elements, $|\gamma| \leq 1$.Note that $p, q = 1, 2, \ldots, N_t$ if $X = \text{tx}$, otherwise $p, q = 1, 2, \ldots, N_r$.

Another arrangement of antenna array is a square antenna array at the transmitter, which is illustrated in Fig. 4.2(b), where d denotes the spacing between adjacent antenna elements. For the sake of brevity, we consider the angle of arrival of the uniform distribution. For example, when the transmitter employs $N_t = 4$ antenna elements, the transmitter correlation matrix of the square antenna array is given by [35]:

$$\Sigma_{\text{tx}} = \begin{bmatrix} 1 & J_0(\beta) & J_0(\sqrt{2}\beta) & J_0(\beta) \\ J_0(\beta) & 1 & J_0(\beta) & J_0(\sqrt{2}\beta) \\ J_0(\sqrt{2}\beta) & J_0(\beta) & 1 & J_0(\beta) \\ J_0(\beta) & J_0(\sqrt{2}\beta) & J_0(\beta) & 1 \end{bmatrix}, \tag{4.3}$$

where $\beta = 2\pi d/\lambda$ with λ denoting the carrier wavelength and $J_0(\cdot)$ is the zeroth-order Bessel function of the first kind.

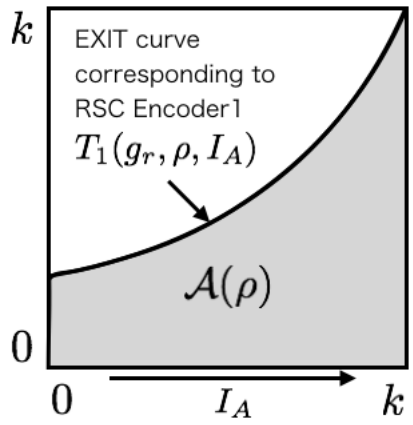

Figure 4.3: The area $\mathcal{A}(\rho)$.

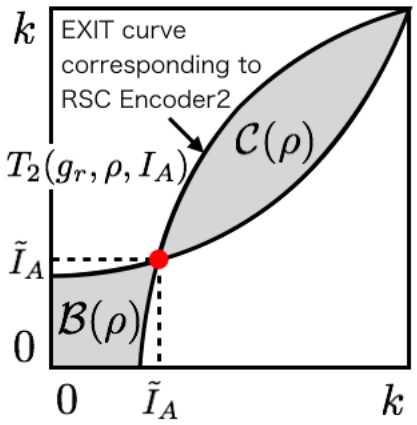

Figure 4.4: The areas $\mathcal{B}(\rho)$ and $\mathcal{C}(\rho)$.

4.2.3 Receiver

In the demapper of SM-TTC, the metric for symbol-based log maximum *a posteriori* (log-MAP) decoder $\mathbf{m}(t) = [m_0, \ldots, m_{N_t M-1}]$ is calculated as follows:

$$m_i = -\frac{\|\mathbf{y}(t) - \mathbf{H}(t)\mathbf{x}^{(i)}(t)\|^2}{\sigma_n^2}, \tag{4.4}$$

where $\mathbf{x}^{(i)}(t)$ is the transmitted signal which can be obtained from the index i determined by the output of the channel encoder. The metric $\mathbf{m}(t)$ is fed into the log-MAP decoder to recover $\tilde{\mathbf{u}}(t)$, which is an estimate of the information bit sequence $\mathbf{u}(t)$. The iterative decoding structure of Fig. 4.1 includes two component decoders using the symbol-based log-MAP algorithm as in [30]. The log-MAP decoder computes the log-likelihood ratio (LLR) for each information bit sequence $\mathbf{u}(t)$ for $j = 0, 1, \ldots, 2^k - 1$, as follows:

$$L_p(\mathbf{u}(t) = j) = \ln \frac{p[\mathbf{u}(t) = j|\mathbf{m}(t)]}{p[\mathbf{u}(t) = 0|\mathbf{m}(t)]}. \tag{4.5}$$

The integer j with the largest LLR in (4.5) is chosen as the decimal scalar of $\tilde{\mathbf{u}}(t)$.

4.3 Code Search Method

4.3.1 Symbol-base EXIT Charts

Symbol-based EXIT charts [31, 36] allow us to study the convergence of iterative decoding of nonbinary codes and TTCM. We assume that the interleaver is sufficiently long to neglect tail effects (open/terminated trellises of convolutional codes) and the *extrinsic* information for each bit/symbol is mutually independent, as in [36]. Moreover, this method has to generate the *a priori* input of the log-MAP decoder and to calculate the average *extrinsic* information. In this paper, the process of generating the *a priori* input is the same as in [36]. Furthermore, in order

Algorithm 2 Proposed code search method

Require: G_r (The set of the feed-back GPs)
ρ_{l} (The minimum of ρ)
ρ_{r} (The maximum of ρ)
ϵ (The threshold of Bisection Method)
Ensure: $\hat{g}_r$ (The feed-back GP of the best code)

```
for g_r ∈ G_r do
    ρ_1 := ρ_l and ρ_2 := ρ_r
    repeat
        ρ := (ρ_1 + ρ_2)/2
        Compute f(ρ) := 2A(ρ) − k^2
        if f(ρ) < 0 then
            ρ_1 := ρ
        else
            ρ_2 := ρ
        end if
    until |f(ρ)| < ε
    ρ̃_{g_r} := ρ
end for
return ĝ_r = arg min_{g_r} {ρ̃_{g_r}}
```

to reduce the computational complexity, the average *extrinsic* information is calculated as in [37].

4.3.2 Conventional Code Search

The code search algorithm, which finds the best code for TTCM using symbol-based EXIT charts [36], has been proposed in [32]. In the rest of this paper, the GP of the component code is denoted by $[g_r \ g_1 \ \dots \ g_k]$, where g_r denotes the feed-back GP. In addition, the set of the feed-back GPs which can be candidate is denoted by G_r. The algorithm can simply find the best code for TTCM by finding the GP g_r, which results in an open EXIT-tunnel at the lowest SNR $\tilde{\rho}_{\mathrm{conv.}}$. Furthermore, the code search using the algorithm is a search in a one-dimensional continuous space along the SNR axis. However, its computational complexity is considerably high, since the algorithm needs iterative decoding to track the EXIT trajectory.

4.3.3 Proposed Code Search

We derived a method for finding the best component code, which is listed in Algorithm 1. As with the search method of [32], our proposal is a search in a one-dimensional continuous space along the SNR axis and requires the set G_r.

In our method, for any SNR ρ, the function

$$f(\rho) = 2\mathcal{A}(\rho) - k^2, \tag{4.6}$$

Table 4.1: The value of $\tilde{\rho}$ and GPs for SM-TTC.

Scenario/ (N_t, N_r)	GP (Octal) $[g_r\ g_1\ g_2\ g_3]$		$\tilde{\rho}$ [dB]	
	proposed	[27]	proposed	[27]
Scenario1/(8,2)	[15 2 4 10]	[11 2 4 10]	5.23	5.29
Scenario2/(4,2)	[15 2 4 10]	[11 2 4 10]	5.13	5.20

has to be evaluated, where $\mathcal{A}(\rho)$ is the area shown in Fig. 4.3. Furthermore, using the areas $\mathcal{B}(\rho)$ and $\mathcal{C}(\rho)$ shown in Fig. 4.4, $f(\rho)$ can be also expressed as

$$f(\rho) = \mathcal{B}(\rho) - \mathcal{C}(\rho), \tag{4.7}$$

since the two component codes are identical.

Let $T_1(g_r, \rho, I_A)$ denote the EXIT curve corresponding to RSC encoder1 with g_r, which is a function of the SNR ρ and of the *a priori* information I_A. Then, $T_1(g_r, \rho, I_A)$ is a monotonically increasing function of both I_A and ρ, and its shape depends on g_r [38]. Hence, for any SNR ρ, $\mathcal{B}(\rho)$ and $\mathcal{C}(\rho)$ can be regarded as monotonically increasing and decreasing functions, respectively. Moreover, let $\tilde{I}_A$ be the crossover point of the pair of EXIT curves corresponding to RSC encoder 1 and 2, i.e., $T_1(g_r, \rho, I_A)$ and $T_2(g_r, \rho, I_A)$. When $\tilde{I}_A$ approaches its maximum value k with a high gradient - where k is the number of information bits - an open EXIT-tunnel is expected to emerge for a smaller ρ. Furthermore, if $\tilde{I}_A$ increases with a high gradient, $\mathcal{B}(\rho)$ is also increased sharply since $\mathcal{B}(\rho)$ is given by $\mathcal{B}(\rho) = 2\int_0^{\tilde{I}_A} T_1(g_r, \rho, I_A) dI_A - \tilde{I}_A^2$. Therefore, if $\mathcal{B}(\rho)$ becomes equal to $\mathcal{C}(\rho)$ at a lower ρ, this event corresponds to one having an open tunnel at a lower ρ, hence the best code can be found by evaluating $\tilde{\rho} := \{\rho | f(\rho) = 0\}$ instead of evaluating the EXIT trajectories.

In order to further reduce the computational complexity to search for the best code, we seek the value of $\tilde{\rho}$ by the classic bisection method. Then, we need a pair of SNR values ρ_{l} and ρ_{r}, which satisfy $f(\rho_{\mathrm{l}}) < 0$ and $f(\rho_{\mathrm{r}}) \geq 0$, respectively. In our method, the value of $\tilde{\rho}$ is evaluated for $g_r \in G_r$. The specific code, which has the minimum value of $\tilde{\rho}$, is deemed to be the best feed-back GP $\hat{g}_r$.

From these above mentioned, there are three differences between our proposal and conventional method:

- Using the areas obtained from EXIT chart instead of EXIT trajectory.
- There is no need to execute iterative decoding.
- The order of the convergence of the calculation of the metric is linear.

4.4 Numerical Results

4.4.1 Results of Code Search

We investigate the best codes and BER performances of SM-TTC for Scenario1 and Scenario2, where all antenna elements are equally spaced on a straight line. In Scenario1 SM-TTC employs $N_t = 8$ TA elements, $N_r = 2$ RA elements, and binary phase shift keying (BPSK). By contrast,

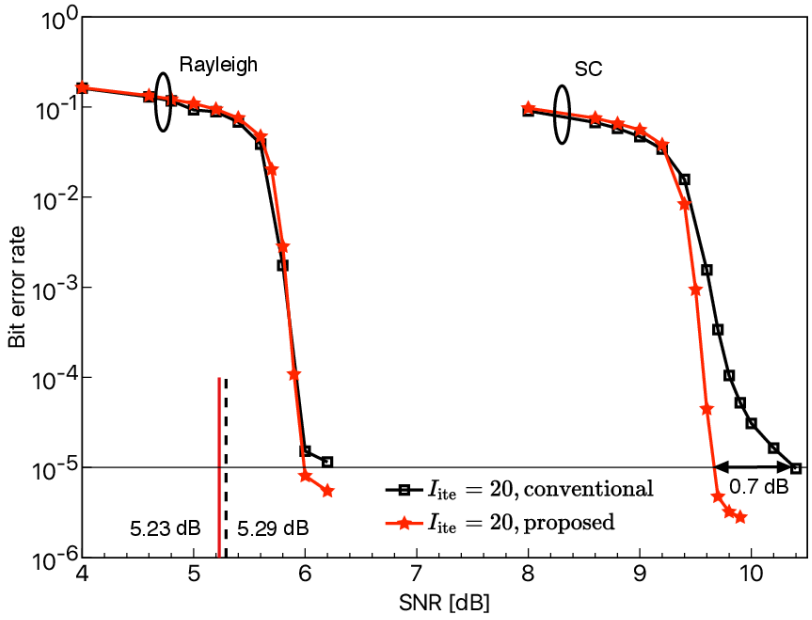

Figure 4.5: The BER performances of SM-TTC employing the linear antenna array in Scenario1. The correlation coefficient γ is 0.8.

in Scenario2 $(N_t, N_r) = (4, 2)$ and QPSK is used. In both scenarios, the transmission rate and the codeword length are 3 bpcu and 10,000 symbols, respectively. The number of decoding iterations is denoted by I_{ite}.

Table 4.1 lists the GPs of the best codes in Rayleigh fading channels and their values of $\tilde{\rho}$, where $\epsilon = 0.01$. The values of $\tilde{\rho}$ of the code used in [27] are also listed in Table 4.1. According to Table 4.1, our best code only outperforms the code of [27] by 0.06 dB in Scenario1 and by 0.07 dB in Scenario2.

4.4.2 BER Performance

The BER performances of SM-TTC employing the linear antenna array in Scenario1 are shown in Fig. 4.5, where we use $I_{\text{ite}} = 20$ for transmission over Rayleigh fading channels and SC channels with $\gamma = 0.8$. The associated values of $\tilde{\rho}$ are also shown in Fig. 4.5. Observe that the error floor is lower for transmission over Rayleigh fading channels. Moreover, at a BER of 10^{-5}, the result indicates that our code performs about 0.7 dB better than the code of [27] for transmission over SC channels.

Figure 4.6 shows the BER performances of SM-TTC employing the linear antenna array and the associated values of $\tilde{\rho}$ in Scenario2, where we use $I_{\text{ite}} = 20$ for transmission over Rayleigh fading and SC channels with $\gamma = 0.8$. According to Fig. 4.6, it turns out that the performances of SM-TTC over both Rayleigh fading and SC channels are improved using our code. In particular, it is predicted that our code outperforms the code of [27] by about 0.8 dB over SC channels, at a BER of 10^{-5}.

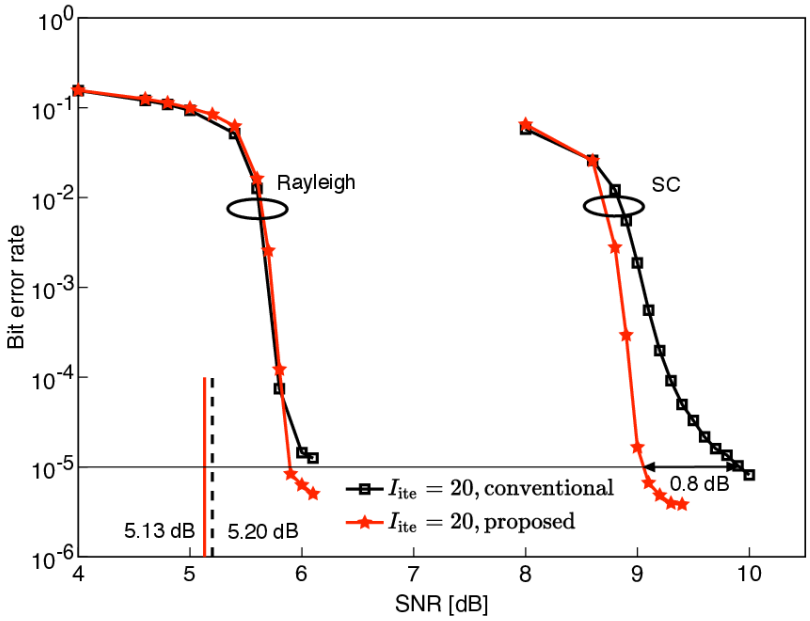

Figure 4.6: The BER performances of SM-TTC employing the linear antenna array in Scenario2. The correlation coefficient γ is 0.8.

Finally, the BER performances of SM-TTC employing $N_t = 4$ TA elements, $N_r = 2$ RA elements, and QPSK, in SC channels with d/λ of 0.1 at the transmitter and 0.5 at the receiver, are shown in Fig. 4.7. Here, we consider the square arranged antenna array at the transmitter and use $I_{\text{ite}} = 20$ for the transmission. Moreover, the receiver correlation matrix is given by

$$\Sigma_{\text{rx}} = \begin{bmatrix} 1 & J_0(\beta_{\text{rx}}) \\ J_0(\beta_{\text{rx}}) & 1 \end{bmatrix}, \tag{4.8}$$

where β_{rx} denotes the value of β at the receiver. Our code outperforms the code of [27] by about 1.0 dB at a BER of 10^{-5}. This result implies that SM-TTC using our code can obtain higher gain than conventional one when the transmitter correlation is more serious.

4.4.3 Computational Complexity

We also investigate the computational complexity of code searth methods. Unfortunately, since both of the proposed and conventional code search methods are based on Monte Carlo method, we evaluate the average executing time. We observe the time to calculate $\mathcal{A}(\rho)$ in our proposal and the time to confirm whether the tunnel between two EXIT curves appears or not in the conventional search.

The results for Scenario2 are shown in Fig. 4.8. Note that the time to calculate $\mathcal{A}(\rho)$ is independent on the value of SNR ρ. Figure 4.8 indicates that the conventional search needs twice as more time for one processing as our proposal in the waterfall region, cf. Fig. 4.6. Furthermore, the average executing time of the conventional scheme is higher than our proposal

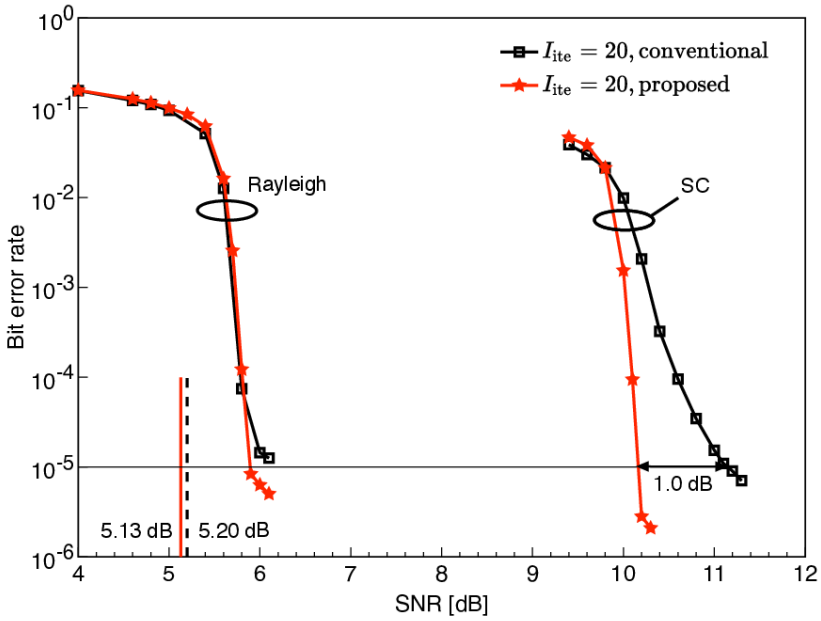

Figure 4.7: The BER performances of SM-TTC employing the square antenna array at the transmitter where we use $N_t = 4$ TA elements with $d/\lambda = 0.1$ and $N_r = 2$ RA elements with $d/\lambda = 0.5$. The associated performances in Scenario2 for transmission over Rayleigh fading channels are also shown.

in SNE region between 5.0 dB to 6.5 dB. These facts imply that our proposal can significantly reduce the computational complexity of the entire searching process, since the conventional search strictly seeks the minimum SNR, which the tunnel between two EXIT curves appears, with changing the value of SNR.

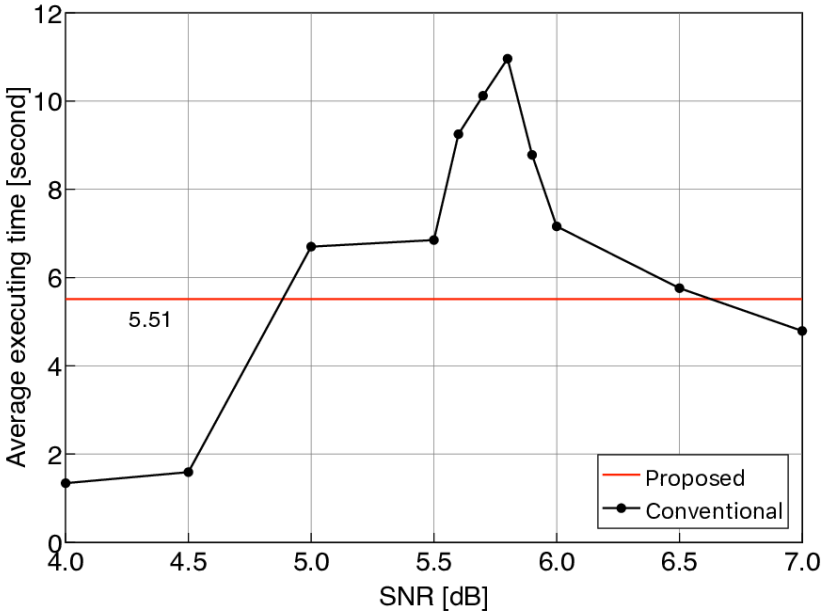

Figure 4.8: The average computational complexity versus the value of SNR ρ for Scenario2. The red line and block line are the time to calculate $\mathcal{A}(\rho)$ and the time to confirm whether the tunnel between two EXIT curves appears or not, respectively.

4.5 Chapter Summary

In this chapter, for improving the BER performance of SM over SC channels, we have proposed a code search method using symbol-based EXIT charts and the bisection method. We reviewed the SM-TTC system and introduced code search methods briefly. After we showed that SM-TTC using the code found by our proposal outperforms the conventional SM-TTC from the approximated performance limit, we confirmed that the BER performance of our SM-TTC is superior to that of the conventional one via computer simulations. Finally, we evaluated the computational complexity of code search methods and the result indicated that the proposed method can significantly reduce the complexity as compared to the conventional method.

Chapter 5

Conclusions and Future Works

We have comprehensively investigated the SM systems, i.e., multiuser SM and CSM, for mMTC and eMBB scenarios. Conclusions and contributions of this thesis are summarized below.

The contribution of this thesis consists of two parts. In the first part (chapter 3), we assumed a simple multiuser SM system using random access and proposed the algorithm for the channel estimation, called *block-sparse complex message passing*. We also demonstrated that the accuracy of channel estimation by the proposed algorithm is enough to achieve almost ideal effective throughput performance in the multiuser SM system via computer simulations.

On the other hand, in the second part (chapter 4), we assumed the SM system with turbo trellis-coding, i.e., SM-TTC. We addressed the optimization of the performance of SM-TTC and proposed the low-complexity code search method for SM-TTC. From the simulation results, it is confirmed that SM-TTC with the code obtained by the proposed code search outperforms the conventional one over both spatially uncorrelated and correlated channels. In particular, the outstanding improvement of the performance could be obtained against spatially correlated channels.

From these works, we may conclude that this thesis provided a simple framework of the design of multiuser SM system including channel estimation and an approach for the performance degradation of SM system by spatial correlation of channels.

However, there still exist a lot of challenges. For example, the performance analysis and the optimization of the proposed algorithm have not been addressed and the channel estimation error is not considered in the comprehensitive design of multiuser SM system. Furthermore, we only tried the optimization of SM-TTC in a specific setup, however, the system with a higher transmission rate should be considered in order to realize the system for eMBB. Therefore, we list the future works as follows:

- The optimization and analysis of BS-CAMP.
- The design of the joint channel estimation and MUD for multiuser SM systems.
- The design of GSM with turbo trellis-coding and the high-rate CSM systems.

References

[1] "Framework and overall objectives of the future development of imt for 2020 and beyond," document ITU-R M.2083-0, International Telecommunication Union (ITU), Feb. 2015.

[2] "The road to 5g: drivers, applications, requirements and technical development," Global mobile Suppliers Association and others, Nov. 2015.

[3] L. D. Xu, W. He, and S. Li, "Internet of things in industries: a survey," *IEEE Trans. Ind. Informat.*, vol. 10, no. 4, pp. 2233–2243, Nov. 2014.

[4] L. Liu, E. G. Larsson, W. Yu, P. Popovski, C. Stefanovic, and E. de Carvalho, "Sparse signal processing for grant-free massive connectivity: a future paradigm for random access protocols in the internet of things," *IEEE Signal Processing Mag.*, vol. 35, no. 5, pp. 88–99, Sep. 2018.

[5] Y. Saito, Y. Kishiyama, A. Benjebbour, T. Nakamura, A. Li, and K. Higuchi, "Non-orthogonal multiple access (NOMA) for cellular future radio access," in *Proc. 2013 IEEE 77th Vehicular Technology Conference (VTC-Spring)*, Dresden, Germany, 2013, pp. 1–5.

[6] R. Mesleh, H. Haas, S. Sinanovic, C. W. Ahn, and S. Yun, "Spatial modulation," *IEEE Trans. Veh. Technol.*, vol. 57, no. 4, pp. 2228–2241, Jul. 2008.

[7] M. D. Lenzo, H. Haas, A. Ghrayeb, S. Sugiura, and L. Hanzo, "Spatial modulation for generalized MIMO: challenges, opportunities, and implementation," *Proc. IEEE*, vol. 102, no. 1, pp. 56–103, Jan. 2014.

[8] K. Ishibashi and S. Sugiura, "Effects of antenna switching on band-limited spatial modulation," *IEEE Wireless Commun. Lett.*, vol. 3, no. 4, pp. 345–348, Aug. 2014.

[9] A. Younis, N. Serafimovski, R. Mesleh, and H. Haas, "Generalised spatial modulation," in *Proc. 2010 44th Asilomar Conf. on Signals, Systems and Computers*, Pacific Grove, CA, USA, 2010, pp. 1498–1502.

[10] M. K. Simon and M.-S. Alouini, *Digital Communication over Fading Channels*, 2nd ed. John Wiley & Sons, Inc., 2005.

[11] S. X. Ng and L. Hanzo, "On the MIMO channel capacity of multidimensional signal sets," *IEEE Trans. Veh. Technol.*, vol. 55, no. 2, pp. 528–536, Mar. 2006.

[12] P. Raviteja, T. L. Narasimhan, and A. Chockalingam, "Large-scale multiuser SM-MIMO versus massive MIMO," in *Proc. 2014 Information Theory and Applications Workshop (ITA)*, San Diego, CA, USA, 2014, pp. 1–9.

[13] X. Menga, S. Wu, L. Kuang, D. Huang, and J. Lu, "Multi-user detection for spatial modulation via structured approximate message passing," *IEEE Commun. Lett.*, vol. 20, no. 8, pp. 1527–1530, Aug. 2016.

[14] S. Wang, Y. Li, M. Zhao, and J. Wang, "Energy-efficient and low-complexity uplink transceiver for massive spatial modulation MIMO," *IEEE Trans. Veh. Technol.*, vol. 64, no. 10, pp. 4617–4632, Oct. 2015.

[15] Y. Liu, L.-L. Yang, and L. Hanzo, "Spatial modulation aided sparse code-division multiple access," *IEEE Trans. Wireless Commun.*, vol. 17, no. 3, pp. 1474–1487, Mar. 2018.

[16] T. Wang, S. Liu, F. Yang, J. Wang, J. Song, and Z. Han, "Generalized spatial modulation-based multi-user and signal detection scheme for terrestrial return channel with noma," *IEEE Trans. Broadcast.*, vol. 64, no. 2, pp. 211–219, Jun. 2018.

[17] Z. Ding, X. Lei, G. K. Karagiannidis, R. Schober, J. Yuan, and V. K. Bhargava, "A survey on non-orthogonal multiple access for 5g networks: research challenges and future trends," *IEEE J. Sel. Areas Commun.*, vol. 35, no. 10, pp. 2181–2195, Oct. 2017.

[18] Y. Du, W. Zhou, K. Gao, C. Chen, X. Wang, and J. Fang, "Joint channel estimation and multiuser detection for uplink grant-free NOMA," *IEEE Wireless Commun. Lett.*, vol. 7, no. 4, pp. 682–685, Aug. 2018.

[19] L. Anitori, A. Maliki, M. Otten, R. G. Baraniuk, and P. Hoogeboom, "Design and analysis of compressed sensing radar detectors," *IEEE Trans. Signal Process.*, vol. 61, no. 4, pp. 813–827, Feb. 2013.

[20] D. L. Donoho, I. Johnstone, and A. Montanari, "Accurate prediction of phase transitions in compressed sensing via a connection to minimax denoising," *IEEE Trans. Inf. Theory*, vol. 59, no. 6, pp. 3396–3433, Feb. 2013.

[21] M. Thill and B. Hassibi, "Low-coherence frames from group fourier matrices," *IEEE Trans. Inf. Theory*, vol. 63, no. 6, pp. 3386–3404, Jun. 2017.

[22] Y. C. Elder, P. Kuppinger, and H. Bölcskei, "Block-sparse signals: uncertainty relations and efficient recovery," *IEEE Trans. Signal Process.*, vol. 58, no. 6, pp. 3042–3054, Jun. 2010.

[23] R. Mesleh, M. D. Renzo, H. Haas, and P. M. Grant, "Trellis coded spatial modulation," *IEEE Trans. Wireless Commun.*, vol. 9, no. 7, pp. 2349–2361, Jul. 2010.

[24] E. Basar, U. Aygolu, and E. Panayirci, "New trellis code design for spatial modulation," *IEEE Trans. Wireless Commun.*, vol. 10, no. 8, pp. 2670–2680, Aug. 2011.

[25] M. Koca and H. Sari, "Bit-interleaved coded spatial modulation," in *Proc. IEEE 23rd International Symposium on Personal, Indoor and Mobile Radio Communications (PIMRC)*, Sydney, NSW, Australia, 2012, pp. 1949–1954.

[26] C. Vladeanu, "Turbo trellis-coded spatial modulation," in *Proc. IEEE Global Communications Conference (GLOBECOM)*, Anaheim, CA, USA, 2012, pp. 4024–4029.

[27] ——, "Spatial modulation with joint antenna index and symbol index turbo trellis coding," in *Proc. ISSCS 2013 International Symposium on Signals, Circuits and Systems*, Iasi, Romania, 2013, pp. 1–4.

[28] G. Ungerboeck, "Channel coding with multilevel/phase signals," *IEEE Trans. Inf. Theory*, vol. 28, no. 1, pp. 55–67, Jan. 1982.

[29] G. Caire, G. Taricco, and E. Biglieri, "Bit-interleaved coded modulation," *IEEE Trans. Inf. Theory*, vol. 44, no. 3, pp. 927–946, May 1998.

[30] P. Robertson and T. Wörz, "Bandwidth-efficient turbo trellis-coded modulation using punctured component codes," *IEEE J. Sel. Areas Commun.*, vol. 16, no. 2, pp. 206–218, Feb. 1998.

[31] A. Grant, "Convergence of non-binary iterative decoding," in *Proc. Global Telecommunications Conference (GLOBECOM)*, San Antonio, TX, USA, 2001, pp. 1058–1062.

[32] S. X. Ng, O. R. Alamri, Y. Li, J. Kliewer, and L. Hanzo, "Near-capacity turbo trellis coded modulation design based on EXIT charts and union bounds," *IEEE Trans. Commun.*, vol. 56, no. 12, pp. 2030–2039, Dec. 2008.

[33] A. Forenza, D. Love, and R. W. Heath Jr., "A low complexity algorithm to simulate the spatial covariance matrix for clustered MIMO channel models," in *Proc. IEEE Vehicular Technology Conference (VTC-Spring)*, Los Angeles, CA, USA, 2004, pp. 889–893.

[34] S. L. Loyka, "Channel capacity of MIMO architecture using the exponential correlation matrix," *IEEE Commun. Lett.*, vol. 5, no. 9, pp. 369–371, Sep. 2001.

[35] W. Ge, P. Fan, and K. Q. T. Zhang, "Performance analysis of square arranged antenna array with SC and MRC receiver over Nakagami fading channel," *IEEE Trans. Veh. Technol.*, vol. 55, no. 2, pp. 477–489, Mar. 2006.

[36] H. Chen and A. Haimovich, "EXIT charts for turbo trellis-coded modulation," *IEEE Trans. Commun. Lett.*, vol. 8, no. 11, pp. 668–670, Nov. 2004.

[37] J. Kliewer, S. X. Ng, and L. Hanzo, "Efficient computation of EXIT functions for nonbinary iterative decoding," *IEEE Trans. Commun.*, vol. 54, no. 12, pp. 2133–2136, Dec. 2006.

[38] S. T. Brink, "Convergence behavior of iteratively decoded parallel concatenated codes," *IEEE Trans. Commun.*, vol. 49, no. 10, pp. 1727–1737, Oct. 2001.

Acknowledgments

This thesis consists of my master study at the University of Electro-Communications, Tokyo, Japan. I am grateful to a large number of people who have helped me to accomplish my work.

First of all, I would like to express my deepest gratitude to my supervisor, Associate Prof. Koji Ishibashi, for guiding throughout my work. His motivations and encouragements immensely helped me for three years. He also gave me the chance to study abroad for challenging to research in the foreign laboratory, and this experience was invaluable for me. I also would like to give my special thanks to Prof. Yasushi Yamao, Takeo Fujii, and Associate Prof. Koichi Adachi for their valuable guidance, instructions, and continuous support.

I would particularly like to thank Mr. Razvan-Andrei Stoica, who is Ph. D student of Jacobs University Bremen, and Prof. Giuseppe Thadeu Freitas de Abreu, who is Prof. of Jacobs University Bremen, for the joint research.

This thesis contains the contributions of our collaborative research with the University of Southampton. During my stay at the university as a short-term academic visitor, I was indebted to Prof. Lajos Hanzo and Associate Prof. Soon Xin Ng. Thanks to their warm and welcoming attitude, I was able to explore a new research topic and to discuss my research. I have been inspired by the eagerness of members of their laboratory for research.

I am also grateful to all the members of advanced wireless communications and research center (AWCC), especially Mr. Manato Takai, Shun Ogata, Kazuya Ohira, and Tatsuhiro Kawaguchi for their discussions and kindness. Finally, I would like to have my family to thank for their words, attitudes, and every support.

List of Publications

International Conference (3)

1. K. Ohira, T. Hara, and K. Ishibashi, "Aggregate-compression-aided subcarrier IQ index modulation," in *Proceedings of 2018 15th Workshop on Positioning, Navigation and Communications (WPNC)*, Bremen, Germany, 25–26 October 2018, 6 pages.

2. T. Hara, K. Ishibashi, S. X. Ng, and L. Hanzo, "Low-complexity generator polynomial search for turbo trellis-coded spatial modulation using symbol-based EXIT charts," in *Proceedings of 2018 10th International Symposium on Turbo Codes and Iterative Information Processing (ISTC)*, Hong Kong, China, 3–7 December 2018, 5 pages.

3. T. Hara, R.-A. Stoica, K. Ishibashi, and G. T. F. de Abreu, "On the sum-rate capacity and spectral efficiency gains of massively concurrent NOMA systems," to appear in *2019 IEEE Wireless Communications and Networking Conference (WCNC)*.

Domestic Conference (3)

1. T. Hara, K. Ishibashi, and L. Hanzo, "Low-complexity code search method for turbo trellis-coded spatial modulation using symbol-based EXIT charts," in *IEICE Technical Report RCS2018-70*, vol. 118, no. 101, June 2018, pp. 95–100.

2. K. Ohira, T. Hara, and K. Ishibashi, "Aggregate-compression-aided subcarrier IQ index modulation with discreteness-aware approximate message passing ," in *IEICE Technical Report RCS2018-128*, vol. 118, no. 125, July 2018, pp. 243–248.

3. T. Hara, K. Ishibashi, R.-A. Stoica, and G. Abreu, "Low-complexity detection via gaussian belief propagation for frame-theoretic non-orthogonal multiple access," in *Proceedings of the Symposium on Information Theory and Its Applications*, December 2018, pp. 188–193.